1996ApJ...459..393N

THE ASTROPHYSICAL JOURNAL, 459:393–412, 1996 March 1
© 1996. The American Astronomical Society. All rights reserved. Printed in U.S.A.

ATTRIBUTES OF PULSES IN LONG BRIGHT GAMMA-RAY BURSTS

J. P. NORRIS,[1] R. J. NEMIROFF,[1,2] J. T. BONNELL,[3] J. D. SCARGLE,[4] C. KOUVELIOTOU,[3,5] W. S. PACIESAS,[5,6] C. A. MEEGAN,[5] AND G. J. FISHMAN[5]

Received 1995 March 13; accepted 1995 September 7

ABSTRACT

We examine the temporal profiles of bright gamma-ray bursts detected by the Burst and Transient Source Experiment on the *Compton Gamma Ray Observatory*. We deconvolve these profiles into pulses using a model-dependent, least-squares pulse-fitting algorithm. The algorithm has been applied to 41 bright gamma-ray bursts with durations longer than ~ 1.5 s, resulting in more than 400 fitted pulses. Temporal profiles with 64 ms resolution are fitted in four energy bands covering ~ 25 keV to > 1 MeV. We use a pulse model with separate rise and decay time constants and a peakedness parameter. Several trends in pulse shape as a function of energy and time of occurrence are apparent: Pulse width distributions are energy dependent, the mode shifting from ~ 600 ms at low energy to ~ 200 at high energy. The distribution of intervals between pulses exhibits a broad maximum near 1 s, presumably a characteristic emission timescale in long bursts. The most frequently occurring pulse shape is intermediate between exponential and Gaussian. Pulses show a tendency to self-similarity across energy bands. We find that average raw pulse shape dependence on energy is approximately power law, with an index of ~ -0.40, consistent with the autocorrelation analysis of Fenimore et al. Burst asymmetry on short time scales results from the tendency for most ($\sim 90\%$) pulses to rise more quickly than they decay, the majority having rise-to-decay ratios of ~ 0.3–0.5, independent of energy. The dominant trend of spectral softening seen in most pulses arises partially from faster onsets at higher energy and longer decays at lower energies, although in addition, pulses sometimes peak earlier in the higher energy bands. We make an important connection between pulse asymmetry, width, and spectral softening: Among pulses for which shape is relatively well determined, the rise-to-decay ratio is unity or less; as this ratio decreases, pulses tend to be wider, the pulse centroid is more shifted to later times at lower energies, and pulses tend to be spectrally softer.

Subject headings: gamma rays: bursts — methods: data analysis

1. INTRODUCTION

Gamma-ray burst temporal profiles are enormously varied: no two bursts have ever been found to have exactly the same temporal and spectral development (Nemiroff et al. 1993). In many bursts the temporal activity is suggestive of a stochastic process. However, some simple bursts with well-separated structures, each comprising a fast rise and an exponential decay (a FRED; see Fishman et al. 1994, The First BATSE catalog), suggests that bursts may consist of fundamental units of emission, or pulses. Yet it is the rule that temporal structures in a burst overlap substantially, making the study of attributes of individual pulses somewhat difficult. A primary purpose of this paper is to demonstrate that there is a high degree of determinism underlying the varied temporal appearances and that this determinism is manifest at the level of the gamma-ray burst pulse. Pulse shape (but not relative pulse position) is deterministic if the complete temporal development of a pulse is predictable from a set of model pulse parameters. It is the variations in pulse widths, intervals between pulses within a given burst, the number of pulses from burst to burst, and, of central importance to the burst physics, the energy dependence of pulse shape which give rise to the heterogeneous burst forms and which appear to be the random elements of the underlying process. However, we show that there are trends and relationships between some of these apparently random variables.

Desai (1981) originally hypothesized that burst profiles consist of temporal structures separated by a characteristic timescale of order 3–5 s. With the good statistics provided by the Burst and Transient Source Experiment (BATSE) on the *Compton Observatory*, we can now perceive in the brighter bursts that these structures are usually composite, consisting of several pulses with separations ~ 300 ms–3 s (Norris et al. 1994b). We find that a possible alternative explanation, that burst profiles comprise noise processes on a continuum of timescales, is not favored.

Some limitations are necessarily inherent in our approach and selection of data. The conclusions we reach are based on measurements of a subset of the bursts detected by BATSE. We analyze relatively bright bursts with durations greater than ~ 1.5 s, recorded with 64 ms temporal resolution and four channel spectral resolution. Analysis of pulses in shorter bursts, using a different data type with much higher resolution, will be the subject of another paper. Although our approach utilizes a sufficient number of pulses to represent adequately the temporal profile of a given burst, most inferences concerning pulse shape are drawn from those fitted pulses which are deemed "separable"; not severely overlapping, as estimated by relative amplitudes of two pulses and the intervening minimum. We utilize only one functional form to represent pulses; however, this pulse model appears sufficiently flexible to afford a parsimonious representation, easily accommodating the range of most pulse shapes and widths.

[1] NASA/Goddard Space Flight Center, Greenbelt, MD 20771.
[2] George Mason University, Fairfax, VA 22030.
[3] Universities Space Research Association.
[4] NASA/Ames Research Center, Moffet Field, CA 94035.
[5] NASA/Marshall Space Flight Center, Huntsville, AL 35812.
[6] University of Alabama in Huntsville, Huntsville, AL 35899.

© American Astronomical Society • Provided by the NASA Astrophysics Data System

1996ApJ...459..393N

We explore several attributes of pulses that can be measured by fitting models to their shapes and studying the parameters of these models as a function of energy. The pulse widths and intervals between pulses are primary attributes, which should ultimately reveal important clues about burst physics. The nature of spectral evolution of temporal structures in bursts has been unresolved for more than a decade (Norris 1983; Norris et al. 1986; Hurley 1991). It has not been clear whether some or all pulse structures in some or all bursts exhibit softening, or even if some structures harden with time. By examining the shape of pulses as a function of energy, we show that spectral softening with time on short timescales arises within individual pulses themselves. Nemiroff et al. (1994) have shown that bursts tend to be time asymmetric on all timescales (see also Link, Epstein & Priedhorsky 1993). We show that asymmetry on short timescales arises from the presence of individually asymmetric pulses. We make an important connection between pulse asymmetry and spectral softening: Among pulses whose shapes are relatively well determined, the ratio of pulse rise time to decay time is unity or less; as this ratio decreases, spectral softening is more pronounced. It is likely that elementary pulses with reversed-FRED shape—exponential rise, fast decay (ERFDs)—are rare or do not exist.

2. ANALYSIS OF PULSE SHAPES

Our aim is to characterize and measure pulse shape as a function of spectral energy band, assuming that pulses with a definitive form, rather than noise components on a continuum of timescales, are the major component of burst emission. For this purpose, we utilized BATSE burst data from the Large Area Detectors (LADs) with 64 ms temporal resolution and four-channel spectral resolution. These data comprise the interval from 2 s prior to instrument trigger time to at least 230 s after trigger. The LAD lower level discriminator edges define the channel boundaries at approximately 25, 55, 115, and 320 keV, the fourth channel being open-ended (for descriptions of the BATSE instrument and data types, see Fishman et al. 1989). These boundaries are averages over the eight BATSE modules. Higher spectral resolution is routinely available (16 channels) at finer temporal resolution (16 ms) commencing at trigger for intervals of 32 s. However, using our present pulse fitting approach (described below), which requires visual interaction to identify candidate pulses, the compromise of more finely dividing the available counts would result in only a few bursts of intensity sufficient to derive useful results. BATSE bursts are often referred to by a unique chronological identifier, the "trigger" number (but not all triggers are caused by cosmic gamma-ray bursts; approximately two-thirds of triggers are caused by other phenomena). To study pulses with the coarser four-channel resolution, we selected for analysis all bursts up to trigger number 2450 with peak intensity greater than 18,000 counts s^{-1}, in the energy range above 25 keV, as measured on 256 ms timescale, with T_{90} durations greater than 1.5 s (see Norris et al. 1995 for description of duration measurements). The T_{90} duration is defined to be the interval between times when 5% and 95% of the burst counts (above background) are accumulated (Kouveliotou et al. 1993). Table 1 lists the 46 bursts found in this subset, identified by their BATSE trigger numbers and ordered by increasing T_{90} duration, along with their peak intensities.

To realize a uniform data set of fitted pulse shapes, we analyzed the burst time profiles using a single functional form for the pulse model. Previous experience indicated that a self-similar shape for all pulses within a burst does not adequately represent the variations from pulse to pulse (Norris et al. 1992); two pulses would be self-similar if one were derived from the other by a constant scaling of the time coordinate. Therefore, we chose a model with more flexibility, with the pulse intensity described by

$$I(t) = A \exp\left[-(|t - t_{\max}|/\sigma_r)^v\right] \quad t < t_{\max}\,,$$
$$= A \exp\left[-(|t - t_{\max}|/\sigma_d)^v\right] \quad t > t_{\max}\,, \qquad (1)$$

where $t_{\max}$ is the time of the pulse's maximum intensity, A; σ_r and σ_d are the rise ($t < t_{\max}$) and decay ($t > t_{\max}$) time constants, respectively; and v is a measure of pulse sharpness, which we refer to as "peakedness" (lower values imply a more peaked pulse). Combined, the parameters σ_r, σ_d, and v permit a wide variation in pulse shape. Note that equation (1) is not differentiable at $t_{\max} = 0$, but this is not a problem for the purposes of representing pulse shapes and total counts within pulses. Other phenomenological pulse models with only five parameters may offer comparable latitude, but this one appears satisfactorily suited for a description of the problem at hand.

It is suspected that many pulses have FRED-like shapes, but clearly it is not proven that all pulses have such a shape. Therefore, freedom to represent symmetric pulses and ratio of rise time to decay time greater than unity is required. This consideration justifes independent rise and decay parameters. Now consider the effect of the peakedness parameter. For $v = 1$ or 2, equation (1) describes a two-sided exponential or Gaussian, respectively. Figure 1 illustrates pulse shapes for these two possibilities, with $\sigma_d/\sigma_r = 2.5$, near the most frequently occurring decay-to-rise ratio, and a full width at half-maximum (FWHM) near the mode (400 ms) in the pulse width distribution for channel 2. Pulse shapes intermediate to those shown in Figure 1 are representative of many pulses in bursts, since the most frequently occurring peakedness lies approximately halfway between Gaussian and exponential, and the average rise-to-decay ratio is approximately independent of both energy and pulse width. Considerably higher values of v ($\gtrsim 4$) result in nearly flat-topped pulses, while lower than unity yield spikier pulses; these extremes apparently occur often, but they may sometimes be attributable to insufficient temporal resolution (spiky pulses) or to broad overlapping structures (flat-topped pulses). Most pulses have FWHM in the range 200–600 ms. Therefore, in many cases the transition across the peak, where the representation abruptly switches from rise to decay, is not well resolved at 64 ms resolution, and we do not obtain detailed information about this part of the pulse. Also, equation (1) is a phenomenological pulse model, only designed to estimate shapes in order to identify gross trends. Pulse shapes as a function of energy band from fits to several bright bursts are illustrated in Norris et al. (1993), where a much abbreviated summary, using the same analysis approach as we use here, was reported.

We developed and applied an interactive graphical IDL routine for fitting pulses in bursts. The routine iteratively spawns a FORTRAN program, Superfit, that performs a least-squares fit to the burst profile for a given model pulse. Superfit attempts to minimize the difference between the model and time profile by adjusting parameter values and

© American Astronomical Society • Provided by the NASA Astrophysics Data System

1996ApJ...459..393N

TABLE 1

BURST SAMPLE

TRIGGER NUMBER	T_{90}[a] (s)	PEAK INTENSITY[b] (K counts s^{-1})	N_{tot} PULSES				N_{sep} PULSES			
			1	2	3	4	1	2	3	4
1664	3.6	25.4	8	8	8	0	1	1	1	0
1709	4.1	46.5	2	2	3	2	0	0	0	0
1683	4.1	21.0	10	10	9	6	0	1	2	2
1025	4.6	42.1	6	6	7	2	0	0	0	0
142[c]	5.0	26.7	11	13	12	5	0	0	0	0
543	5.6	33.4	4	4	4	3	1	2	2	2
2393	6.1	22.0	3	3	2	1	0	0	1	1
1711	6.7	72.1	9	12	13	5	1	1	2	1
2037	7.2	21.1	6	8	7	4	3	3	3	2
1974	7.7	21.0	3	3	3	0	0	0	0	0
1886	8.7	53.1	3	4	6	7	0	0	0	0
105	9.2	44.3	4	4	4	1	0	0	0	0
999	9.2	38.5	2	2	2	2	2	2	2	2
2321	9.7	28.0	16	15	12	4	1	2	2	2
1609	9.7	157.5	5	4	5	3	2	2	2	2
1425	10.2	28.4	7	7	7	4	4	4	4	3
451	10.2	32.1	3	4	4	2	1	1	1	1
1484	11.8	39.5	7	8	7	3	0	0	0	0
2090	13.3	33.3	12	15	14	5	1	2	3	3
2083	13.3	140.7	2	2	2	2	2	2	2	1
467	14.3	22.4	3	3	2	1	1	1	1	1
1625	15.4	99.7	9	11	12	7	1	1	1	1
1141	16.4	35.0	8	9	8	6	0	0	0	0
1473	18.9	84.3	6	9	9	7	1	1	1	0
1085	20.0	94.7	4	4	4	2	0	0	0	0
1122	20.0	46.8	8	10	10	7	0	0	0	0
1663	20.5	80.1	7	13	12	13	0	0	0	0
1157	22.5	34.3	10	10	10	9	1	4	4	3
2329	23.0	126.9	0	0	0	0	0	0	0	0
1440	23.6	44.8	16	16	15	12	8	8	12	7
1541	24.6	97.6	31	36	36	28	4	5	6	6
249	25.1	192.8	12	12	13	13	1	1	1	1
219	25.1	75.7	11	12	11	8	4	4	4	1
1698	28.2	27.0	6	7	7	5	0	0	0	0
841	29.2	19.9	12	12	9	1	2	4	4	1
2067	30.7	53.2	8	8	7	8	0	1	1	1
2450	41.0	24.5	32	30	32	12	0	0	0	0
678	41.0	40.0	0	0	0	0	0	0	0	0
1121	47.1	35.5	10	9	8	6	0	2	2	2
2080	49.2	18.4	0	0	0	0	0	0	0	0
143	50.7	256.4	16	16	15	15	3	3	4	4
2232	51.7	18.8	19	19	18	9	1	3	3	1
2533	56.3	29.7	0	0	0	0	0	0	0	0
2228	71.7	24.3	31	36	40	18	4	5	5	1
1606	89.1	27.5	0	0	0	0	0	0	0	0
2156	154.6	56.0	31	32	31	21	7	7	7	2
Total.....			413	448	440	269	57	73	83	54

[a] Interval between times when 5% and 95% of burst counts (above background) accumulate.
[b] Peak intensity summed over LAD channels 1–4 (> 25 keV).
[c] Coarse estimates for T_{90} duration and peak intensity

tracking the effects of their respective changes on the contributions to χ^2. Superfit employs two methods for converging on the "best" set of parameter values: the Marquardt technique far from convergence, and Gauss-Newton near convergence. Pulse shapes as a function of energy and position within the burst are fitted following a rule-based approach for pulse placement, initial pulse shape estimates, and chronology of parameter constraint: The procedure is initiated by specifying the number of apparent pulses and the approximate positions of their peaks within the burst, plus one or two intervals from which an estimate of the background level is obtained. A first-order polynomial [$I(t) = mt + I_0$] is employed to represent the background. Upon each successful convergence of Superfit, the option to add or delete pulses is allowed. Also, minimum or maximum limits on parameter values may be adjusted, or alternatively, parameter values may be fixed. The latter option is effective for limiting the peakedness parameter from assuming very large values, for instance, in cases in which several low-amplitude pulses overlap and the algorithm is attempting to fit the composite structure with a single broad pulse. The number of pulses is adjusted until the residuals—the difference between data and model as a function of time—are approximately white noise. In cases in which the fit is apparently anomalous, the user may decide to fix other parameter values, but this situation occurs infrequently. One notable exception is that when bursts are too long (six cases) to display the entire profile simultaneously such that

© American Astronomical Society • Provided by the NASA Astrophysics Data System

1996ApJ...459..393N

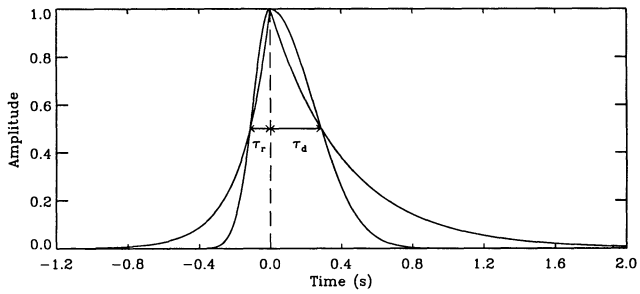

FIG. 1.—Pulse model used to fit all pulse structures in this analysis, evaluated for two values of the peakedness parameter, $n = 1$ or 2, exponential or Gaussian, respectively, and for a rise-to-decay ratio $\sigma_d/\sigma_r = 2.5$. The FWHM for both pulses is 400 ms, near the mode of the pulse width distribution for channel 3. The rise and decay times, half to maximum amplitude, are $\tau_{r,d} = [\ln(2)]^{1/n}\sigma_{r,d}$. Pulse shapes intermediate between the two illustrated are representative of many pulses in bright gamma-ray bursts.

individual pulses are visually resolved, the fit is performed in segments; it is then often necessary to estimate the background in advance and fix the slope and intercept values.

Fits to burst profiles were performed by one investigator and reviewed for accuracy and energy consistency by a second investigator. Throughout this procedure, an attempt was made to associate pulses across energy bands: The fits to all four channels were performed in sequence for each burst. The burst profile was fitted first in the third channel, for which the highest count rates are obtained and pulses are best defined, followed by fits in channels 2, 1, and finally 4, which usually has the lowest count rates. In following this procedure, the primary clue for pulse "reality" was taken from channel 3. The profiles and fits for all four channels were then displayed simultaneously for the investigator to declare the association of separable pulses across energy channels. Because the criterion for separable pulses virtually guarantees that unambiguous temporal alignment of pulse peaks can be made, we consider the results in § 3 which relate information across energy channels to be free of mistaken associations. Obviously, since ~80% of pulses overlap, the same claim could not be made for all pulses.

Several of the fits to burst profiles are shown in the Appendix. These figures illustrate the range of burst appearances, the degree to which fitted pulses are separate or overlap, and the range of acceptability in terms of χ^2. A particularly difficult burst-fitting problem is also apparent in some of these figures: often the wings of a pulse that is embedded within several others will "balloon," thereby artificially subtracting from the counts that would otherwise be fitted by the other pulses. This is the major source of nonuniqueness in our fits and generally appears to be an unsolved problem. Only by assuming a more constrained pulse model can the ambiguity be reduced.

To obtain a sample with the problem of pulse overlap reduced, we identified "separable" pulses among the total sample of fitted pulses. We applied the criterion that the peaks of two overlapping pulses be separated such that the interjacent minimum is at most half the profile intensity at the peak position of the smaller pulse; then about one-fifth of all major pulses may be deemed separable. Table 1 also lists the total number of pulses and the number of "separable" pulses fitted per channel per burst. The number of pulses identifed in channel 4 is about two-thirds that found in channels 1–3, reflecting the lower count rate; in fact, occasionally no pulses are discernible in channel 4. In channel 1 pulse structures are usually wider, and therefore fewer separable pulses are identified.

Five of the 46 bursts were too complex to fit, as indicated by entries of zero pulses in the total pulses column. These are bursts with trigger numbers 678, 1606, 2080, 2329, and 2533. Several attempts were made on each burst, by segmenting the burst profile and fixing several pulse and background parameters. However, the Superfit matrix inversion algorithm, used for the χ^2 minimization, in each case failed to handle the problem of several severely overlapping pulses that appeared necessary for an adequate description. Notice in Table 1 that the average number of total pulses per burst (for successful fits) is 10, whereas no cases occur for which there is only one fitted pulse. If results for the five more complex bursts had been obtained, the average number of pulses would have been higher.

3. ATTRIBUTES OF FITTED PULSES

In this section we describe various attributes of pulses derived from fitting the time profiles. We address these attributes in three categories: pulse shape and relative placement, including width, peakedness, and interval distributions (§ 3.1); energy dependence of pulse shape, including investigations of dependence on rise and decay times and peakedness (§ 3.2); and the connection between pulse asymmetry, width, and spectral hardness (§ 3.3).

3.1. *Pulse Shapes, Widths, and Intervals*

Many derived parameters of burst pulse shapes are best studied preferably using only separable pulses, but some parameters should be investigated for both the whole and separable samples. Figures 2*a*–2*b* illustrate the average,

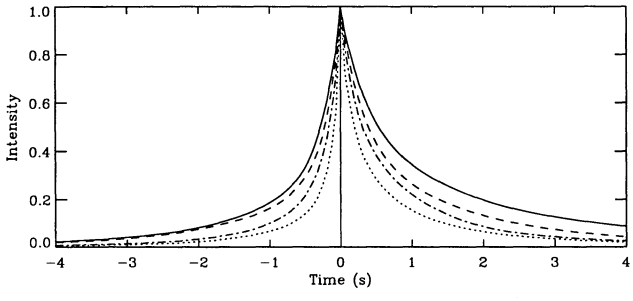

FIG. 2*a*

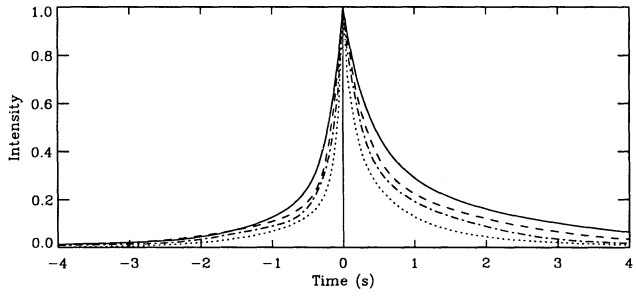

FIG. 2*b*

FIG. 2.—Average pulse shape in energy channels 1 (*solid*), 2 (*dashed*), 3 (*dash-dotted*), and 4 (*dotted*). (*a*) All pulses; (*b*) "separable" pulses only—those whose peaks are sufficiently separated such that the interjacent minimim is at most half the time profile's intensity at peak of the smaller pulse. Separable pulses tend to be 20% (channel 1)–10% (channel 2) narrower than the total sample, whereas the ratios of average pulse widths across channels for the two sets are more comparable (see Table 2).

© American Astronomical Society • Provided by the NASA Astrophysics Data System

1996ApJ...459..393N

TABLE 2

PULSE WIDTHS

CHANNEL	SAMPLE[a]	FULL WIDTH(S) AT NORMALIZED AMPLITUDE[b] 0.2	0.3	0.4	0.5	0.6	0.7	0.8
1	A	2.90	1.79	1.19	0.82	0.56	0.37	0.21
	S	2.22	1.36	0.93	0.66	0.46	0.30	0.18
2	A	2.17	1.34	0.89	0.62	0.43	0.28	0.16
	S	1.64	0.98	0.68	0.49	0.35	0.24	0.15
3	A	1.64	1.06	0.70	0.47	0.32	0.20	0.12
	S	1.38	0.83	0.55	0.39	0.28	0.18	0.11
4	A	1.11	0.68	0.43	0.29	0.19	0.12	0.07
	S	0.96	0.58	0.37	0.26	0.18	0.11	0.07

[a] A = all pulses, S = separable bursts.
[b] Normalized to unity.

peak-aligned pulse shape for these two samples, respectively, for energy channels 1 (*solid*), 2 (*dashed*), 3 (*dash-dotted*), and 4 (*dotted*). The same correspondence between line style and channel is followed in Figures 3–5. The average shapes were generated by summing the fitted pulse profiles in registration at peak intensity, with amplitudes scaled to that of the most intense pulse in each burst. Thus, each burst (not each pulse) is weighted equally (see Fenimore et al. 1995, where the autocorrelations of bursts are weighted equally). The average relative peak intensities in channels 1–4 are 0.45, 0.73, 1.00, and 0.20, respectively. Note that separable pulses tend to be narrower; however, the ratios of average pulse widths across channels for the two sets are nearly equal. The average pulse shapes reflect the well-known trend of narrower pulses at higher energies. Results are summarized in Table 2, which lists the measured values for the average full width of fitted pulses for the four energy channels. The widths are tabulated at amplitudes ranging from 0.2 to 0.8. At normalized amplitudes lower than ~0.2, pulse overlap more severely compromises the measurements; above amplitude of ~0.8, finite temporal resolution limits usefulness of the measurement. Table 3 lists the corresponding ratios of widths between adjacent channels. The error which arises in average pulse shape from sample variation was estimated by randomly selecting half the pulses (but using the same ones in all four energy channels) and averaging. Several such random selections indicate that the variation of pulse shape arising from changes in sample is of the order 10%–15% at each amplitude level.

Following Fenimore et al. (1995), we parameterized the dependence of pulse width on energy channel. Fenimore et al. fitted the autocorrelation functions of portions of profiles near burst peaks, whereas we estimate pulse width in the time domain, at the several amplitude levels listed in Tables 2 and 3. We assumed a power-law dependence of width on energy,

$$W(E) = CE^{-\alpha}, \quad (2)$$

where the choices for E were either the low edges of the energy channels (E_{low}) or the geometric means of low and high edges (E_{mean}). Since the response of the LADs declines very rapidly above 1 MeV, that energy was used as the upper edge for channel 4; the final results are relatively insensitive to the precise value employed, since the average pulse amplitude in channel 4 is much lower than those in the other channels. The fitted power-law indices (α) for the separable and whole samples are summarized in Table 4. Variation in pulse sample (effected by randomly selecting half the pulses as described above) is the dominant source of uncertainty (~10%) in α. Fits for the separable sample yield flatter power laws, by 10%–15%. The average value for α for the whole sample, 0.41, may be compared to that (0.43) found by Fenimore et al. (1995) using the same energy edges and the autocorrelation approach. The determinations using E_{mean} are ~10% lower than those found for E_{low}, similar to the findings of Fenimore et al. However, α is *not* independent of amplitude; for all measures there is a clear trend of steepening power-law index from low to high amplitude, except at amplitude of 0.8, where the values decline by 3%–10% for the various measures (width nearer the peak may be less well determined owing to finite resolution). The average $\Delta\alpha$, from amplitudes 0.2–0.8, is 0.08. Thus, the assumed power-law dependence, as resolved in amplitude in the time domain, appears slightly variable.

There are at least three effects that are most certainly operating to some degree, which tend to bias the fitted pulse shapes in the sense of overestimating pulse widths in the whole sample. First, intrinsically wider pulses clearly tend to overlap to a larger degree, and thus they do not qualify as frequently under our separability criterion as do narrower pulses. Second, the true number of pulses in crowded regions must be underestimated because of pulse overlap. Near-equality of pulse widths in channel 4 for the two samples offers evidence that this is a major factor for the width difference: Since pulses are narrower at higher energy, a larger proportion will be separable, and thus the

TABLE 3

PULSE WIDTH RATIOS

CHANNEL	SAMPLE[a]	RATIO: CHAN{i}/CHAN{i + 1} AT NORMALIZED AMPLITUDE[b] 0.2	0.3	0.4	0.5	0.6	0.7	0.8
1:2	A	1.34	1.33	1.34	1.33	1.32	1.32	1.31
	S	1.36	1.40	1.38	1.34	1.32	1.26	1.22
2:3	A	1.32	1.27	1.26	1.30	1.35	1.40	1.39
	S	1.18	1.17	1.22	1.25	1.25	1.31	1.41
3:4	A	1.47	1.55	1.63	1.65	1.71	1.70	1.57
	S	1.44	1.45	1.48	1.50	1.57	1.65	1.49

[a] A = all pulses, S = separable pulses.
[b] Normalized to unity.

TABLE 4

DEPENDENCE OF PULSE WIDTH ON ENERGY

SAMPLE[a]	⟨α⟩	POWER-LAW INDEX, α, AT NORMALIZED AMPLITUDE[b] 0.2	0.3	0.4	0.5	0.6	0.7	0.8
		$E = E_{low}$[c]						
A	0.41	0.38	0.38	0.40	0.41	0.44	0.46	0.42
S.....	0.36	0.32	0.33	0.35	0.36	0.37	0.40	0.38
		$E = E_{mean}$[c]						
A	0.38	0.35	0.35	0.37	0.38	0.41	0.43	0.39
S.....	0.33	0.30	0.31	0.33	0.33	0.34	0.37	0.36

[a] A = all pulses, S = separable pulses.
[b] Normalized to unity.
[c] E_{low} is low edge of energy channel. E_{mean} is geometric mean of low and high edges; 1 MeV is assumed as upper edge for channel 4.

© American Astronomical Society • Provided by the NASA Astrophysics Data System

1996ApJ...459..393N

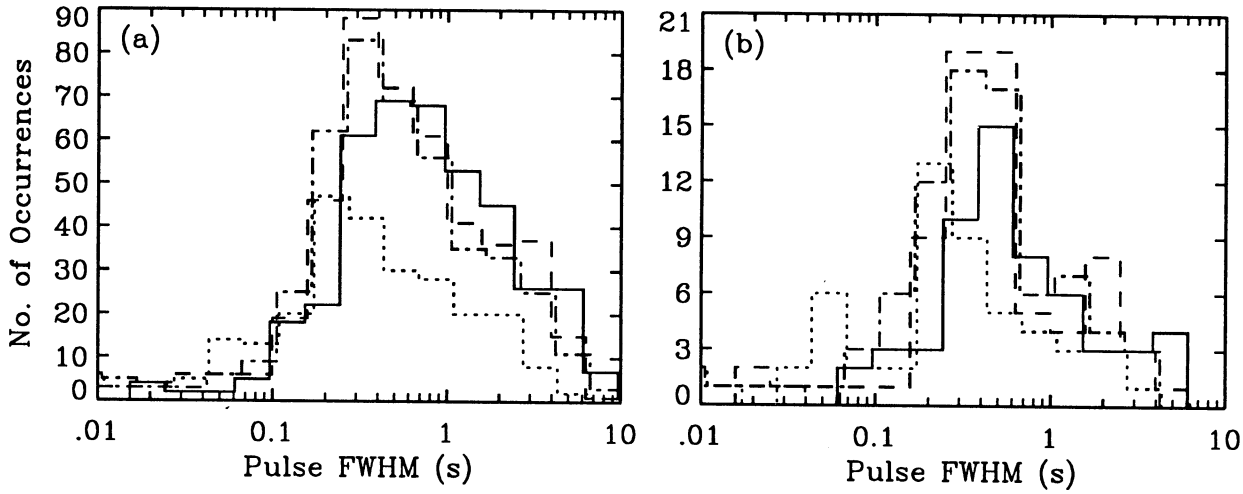

FIG. 3.—Pulse width distributions in the four energy channels, with same correspondence between line style and channel as in Fig. 2. (*a*) All pulses; (*b*) separable pulses only. The majority of pulses have FWHM of a few hundred milliseconds. The well-known trend of narrower pulses at higher energy is apparent in both samples.

two samples will be more nearly equal, leading us to conclude that pulses are not appreciably differently shaped in sparse and crowded regions. This is our main observational justification for presenting many results only for separable pulses. Nevertheless, in regions with several acutely overlapping pulses, our subjective procedure for identifying candidate pulses to be fitted may often result in declaring fewer pulses than are really present, and wider fitted pulses necessarily result, especially in the lower energy channels. Critical evaluation of this effect would be difficult without a more objective pulse identification procedure, especially in the lower energy channels. Third (a more specific example of the first effect), the whole sample includes a small fraction of very long, low-amplitude pulses (usually with high values for v), which are almost always not separable, and these contribute preferentially to the *wings* of the average pulse in the whole sample.

We now examine distributions related to pulse width, clustering, and shape. Notice that distributions for separable pulses will tend to reflect reality more closely for properties that concern width or shape as a function of energy, whereas distributions for the whole sample are more pertinent for total energy considerations and for the important question of the timescale between pulses. Figures 3*a* and 3*b* illustrate pulse width distributions in the four energy channels for all pulses and for separable pulses, respectively. The well-known trend of narrower pulses at higher energy is again apparent in both samples, the mode shifting from ~500–700 ms for channel 1 to ~200 ms for channel 4. If the separable pulses are taken as more reliable width indicators (crowded and sparse regions are not intrinsically different), then we would conclude from Figure 3*b* that the gamma-ray burst phenomenon is dominated by pulses with widths less than 1 s. Figure 3*a* differs in that substantial tails in the distributions are seen to extend to several seconds, but clearly these wider fitted pulses tend to arise in crowded regions where subjective pulse identification is a major concern (more pulses are present than declared).

Figures 4*a*–4*b* illustrate the corresponding distributions for the intervals *between* adjacent pulse peaks. Approximately 80% of the pulse positions are missing in the computation of intervals for Figure 4*b*; it is shown to indicate the proportion of fairly closely spaced, and therefore narrow, pulses which pass the separability criterion. Figure

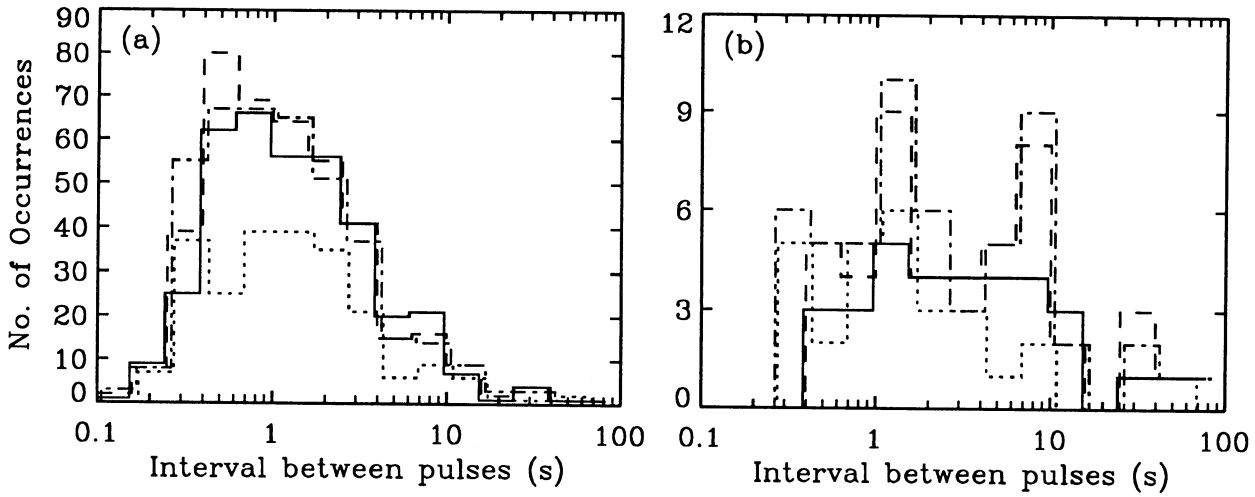

FIG. 4.—Distributions of intervals between pulses in the four energy channels, with same correspondence between line style and channel as in Fig. 2. (*a*) All pulses; (*b*) separable pulses only. In (*a*), the broad mode centered near 1 s reflects the "characteristic timescale" between pulses. Only 20% of intervals survive in (*b*), which is shown merely to indicate the relative proportion of fairly closely spaced, and therefore narrow, separable pulses.

© American Astronomical Society • Provided by the NASA Astrophysics Data System

1996ApJ...459..393N

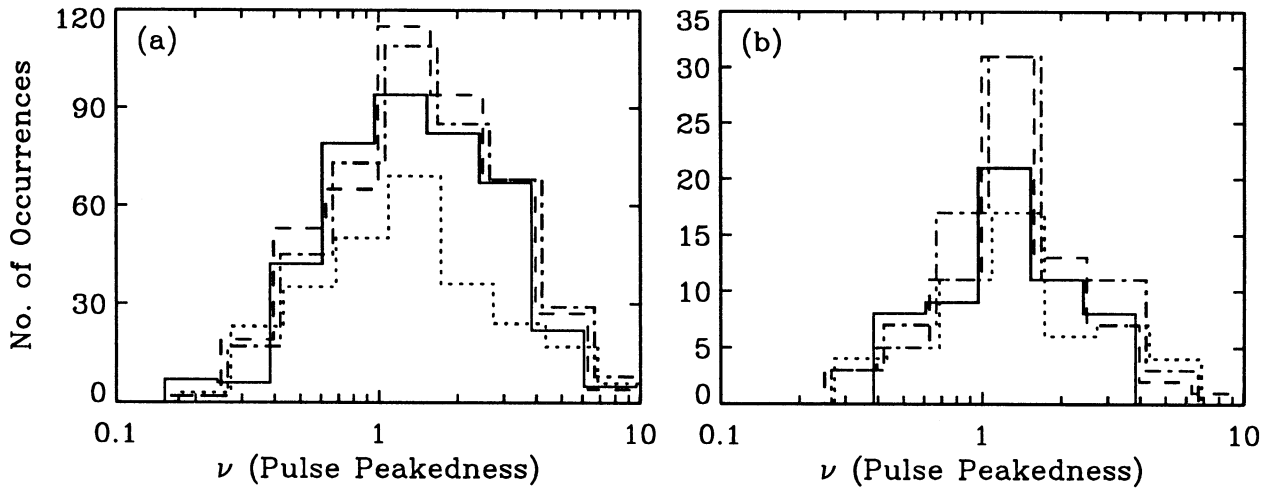

FIG. 5.—Distributions of peakedness parameter, v, in the four energy channels, with same correspondence between line style and channel as in Fig. 2. (*a*) All pulses; (*b*) separable pulses only. Values for v of exactly 1 and 2 correspond to exponential and Gaussian shapes, respectively. Higher values give rise to more flat-topped pulses, lower values to very peaked pulses. In both samples, the mode lies between 1 and 2 for all four channels; for separable pulses, this tendency is accentuated.

4*a* has more interpretative value: Whereas a random distribution of pulse positions would follow Poisson interval statistics (exponentially decreasing form, peaked at zero interval), the measured distribution has a broad maximum centered near 1 s, extending from ~4 s down to ~300 ms, below which it drops sharply. There is probably some underrepresentation of narrow pulses in Figure 4*a* that could be addressed by use of data with higher temporal resolution. However, with 64 ms resolution, at least the peaks of pulses are well enough resolved, and therefore we believe most narrow pulses are identified. We conclude that the interval distribution of Figure 4*a* reflects the "characteristic timescale" between pulses, previously noted by other investigators (Desai 1981; Wood et al. 1986). Thus, among the long bursts analyzed for this study, the mode for the duration of a two-pulse gamma-ray burst will be

$$\tau_{\rm dur} = \text{pulse interval mode} + 2 \times \text{FWHM} \sim 2 \text{ s} , \quad (3)$$

which is near the minimum in the bimodal duration distribution (Kouveliotou et al. 1993). As described in Norris et al. (1994b), the combination of the nonzero mode in the interval distribution for long bursts and the tendency of shorter bursts to have fewer (~60% of short bursts have one or two major pulses), more closely spaced pulses may account naturally for the duration bimodality. More support for this conjecture will require analysis of a larger sample of bursts with durations spanning the short mode (near a few × 100 ms) and the minimum in the duration distribution.

Distributions of the peakedness parameter, v, are plotted in Figures 5*a* and 5*b*. In both samples the mode lies between 1 and 2 for all four channels. For separable pulses, which presumably reflect true shapes more frequently, this tendency for pulse shape to cluster between exponential and Gaussian is accentuated.

3.2. *Pulse Shape Energy Dependence*

First we examine the well-known tendency of pulses to be narrower at higher energies. Quantification of this effect is important not only for understanding the underlying physics of pulses, but also for estimating the correction to apply to the time dilation factor obtained via pulse width measurements (Davis et al. 1994; Norris et al. 1994a; Fenimore & Bloom 1995). Figure 6 illustrates the distributions of ratios of pulse widths between adjacent energy channels for separable pulses only. Nearly all width ratios fall below unity, as expected. The mode shifts from ~0.85 s for the two ratios at lower energies, to ~0.7 for the channel 4:3 ratio. Thus, pulse narrowing is more accentuated in channel 4.

The question immediately arises: Although pulse widths decrease at higher energy, do pulse shapes remain similar across energy bands? This question can be addressed partly by examining the rise-to-decay ratios and peakedness parameters for individual pulses as a function of energy. Assume that equation (1) affords an adequate representation of pulses. Then suppose that a relationship exists between pulse shapes at two energies such that their intensities, both normalized to unity at their respective peaks, are governed by

$$I_1(t) = I_2^K(t) , \quad (4)$$

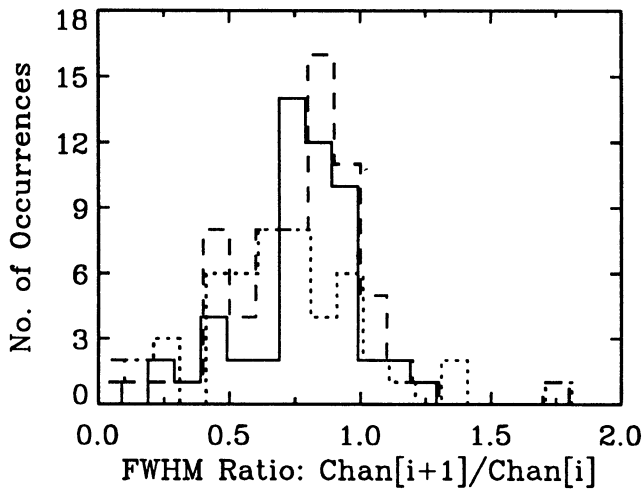

FIG. 6.—Ratios of pulse widths between adjacent energy channels, 2:1 (*solid*), 3:2 (*dashed*), and 4:3 (*dotted*), separable pulses only. Nearly all width ratios fall below unity, reflecting well-known trend of pulse narrowing at higher energies. The mode shifts from ~0.85 s for the two ratios at lower energy to ~0.7 for the 4:3 ratio.

© American Astronomical Society • Provided by the NASA Astrophysics Data System

1996ApJ...459..393N

except for any offset in their times of peak intensity, which we neglect ($t_{max1} = t_{max2}$). Then

$$\exp\left[-(|\Delta t|/\sigma_{r1,d1})^{\nu 1}\right] = \exp\left[-K(|\Delta t|/\sigma_{r2,d2})^{\nu 2}\right], \quad (5)$$

which requires

$$\nu 1 = \nu 2 = \nu, \quad (6a)$$

$$\sigma_{r1}/\sigma_{d1} = \sigma_{r2}/\sigma_{d2}, \quad (6b)$$

$$\sigma_{r1,d1} = K^{-1/\nu}\sigma_{r2,d2}. \quad (6c)$$

If equations (6a) and (6b) hold for a pulse, then the shapes are self-similar in the context of our particular pulse model. In Figures 7–8 the values for ν and for σ_r/σ_d, respectively, are plotted for individual separable pulses for pairs of energy channels to examine how closely the relations in equations (6a) and (6b) are followed. Parameter values for adjacent energy channels are compared in panels (*a*), (*c*), and (*d*) of these Figures for channel pairs 1 and 2, 2 and 3, and 3 and 4, respectively, while panel (*b*) compares channels 1 and 3. Filled (open) symbols indicate pulses for which the peak amplitude is greater (less) than 250 counts per 64 ms bin, in both channels separately. The same meaning for filled and open symbols applies in Figures 9 and 11–14. For bright BATSE bursts, channel 3 routinely records the highest intensity, followed in decreasing order by channels 2, 1, and 4. Considering only the filled symbols, there is a clear trend for pulses to lie near the line of unity slope, indicating *approximately* self-similar shape. Pulses with open symbols have a much larger dispersion in the two figures, with many more occurrences falling away from the line, and with $\sigma_r/\sigma_d > 1.0$ (anti-FREDs), and/or with $\nu > 2.0$ (more flat-topped than a Gaussian). We presume that these pulses with outlying shapes are less accurately measured by our fitting procedure, owing to their lower intensity. The comparison of channels 3 and 4 shows the least tendency toward self-similarity; this lack of definition may be attributable to fewer qualifying pulses of sufficient amplitude and to narrower pulses in the higher energy channels, and therefore fewer points with which to define the pulse shape.

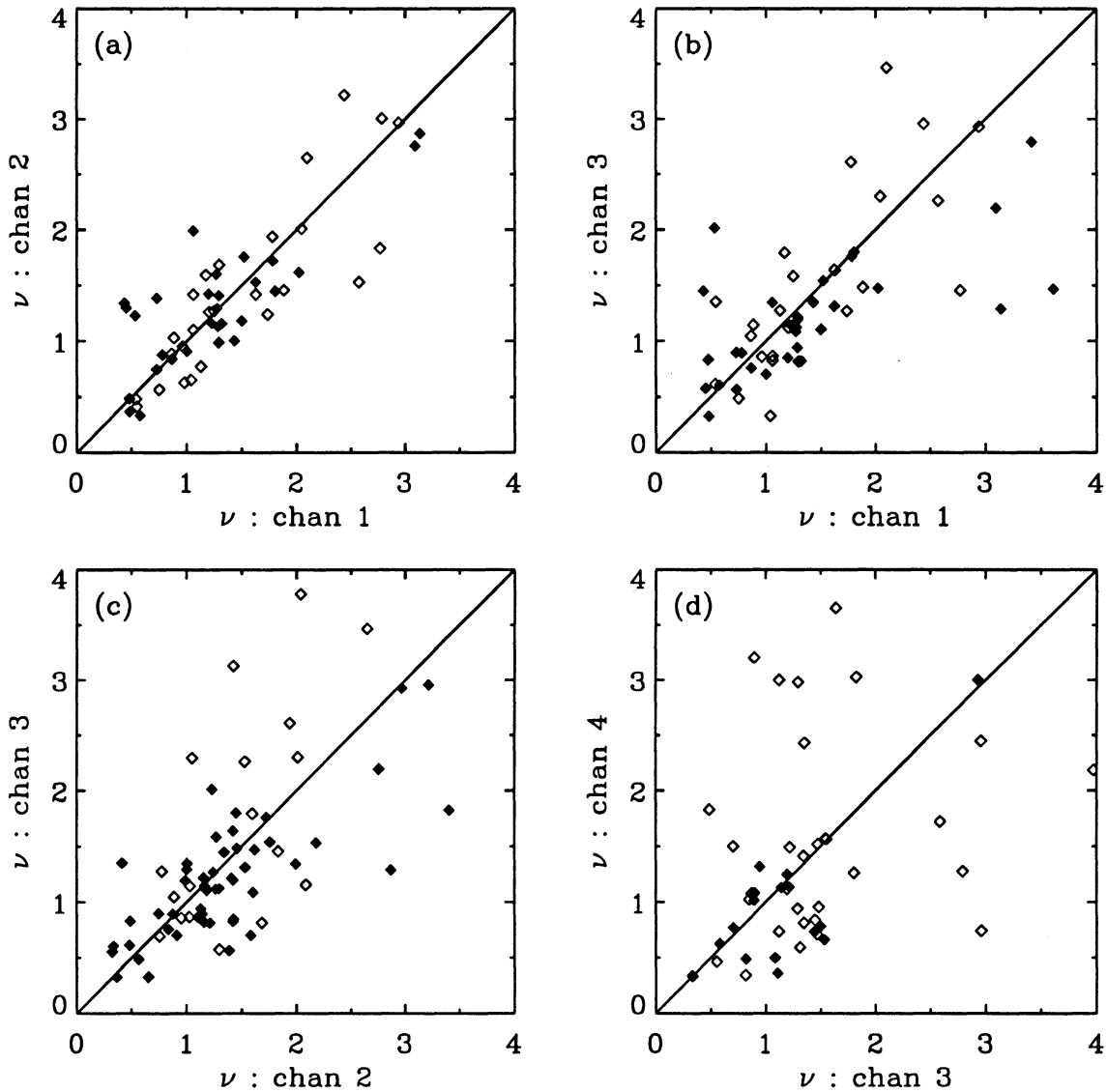

FIG. 7.—Peakedness parameters for separable pulses: (*a*) channels 1 vs. 2, (*b*) 1 vs. 3, (*c*) 2 vs. 3, and (*d*) 3 vs. 4. Any position on line with slope of unity for both peakedness and rise-to-decay ratio (Fig. 8) translates into self-similar pulse shape for compared channels. Filled (open) symbols indicate pulses for which the peak amplitude is greater (less) than 250 counts per 64 ms bin in both channels.

© American Astronomical Society • Provided by the NASA Astrophysics Data System

1996ApJ...459..393N

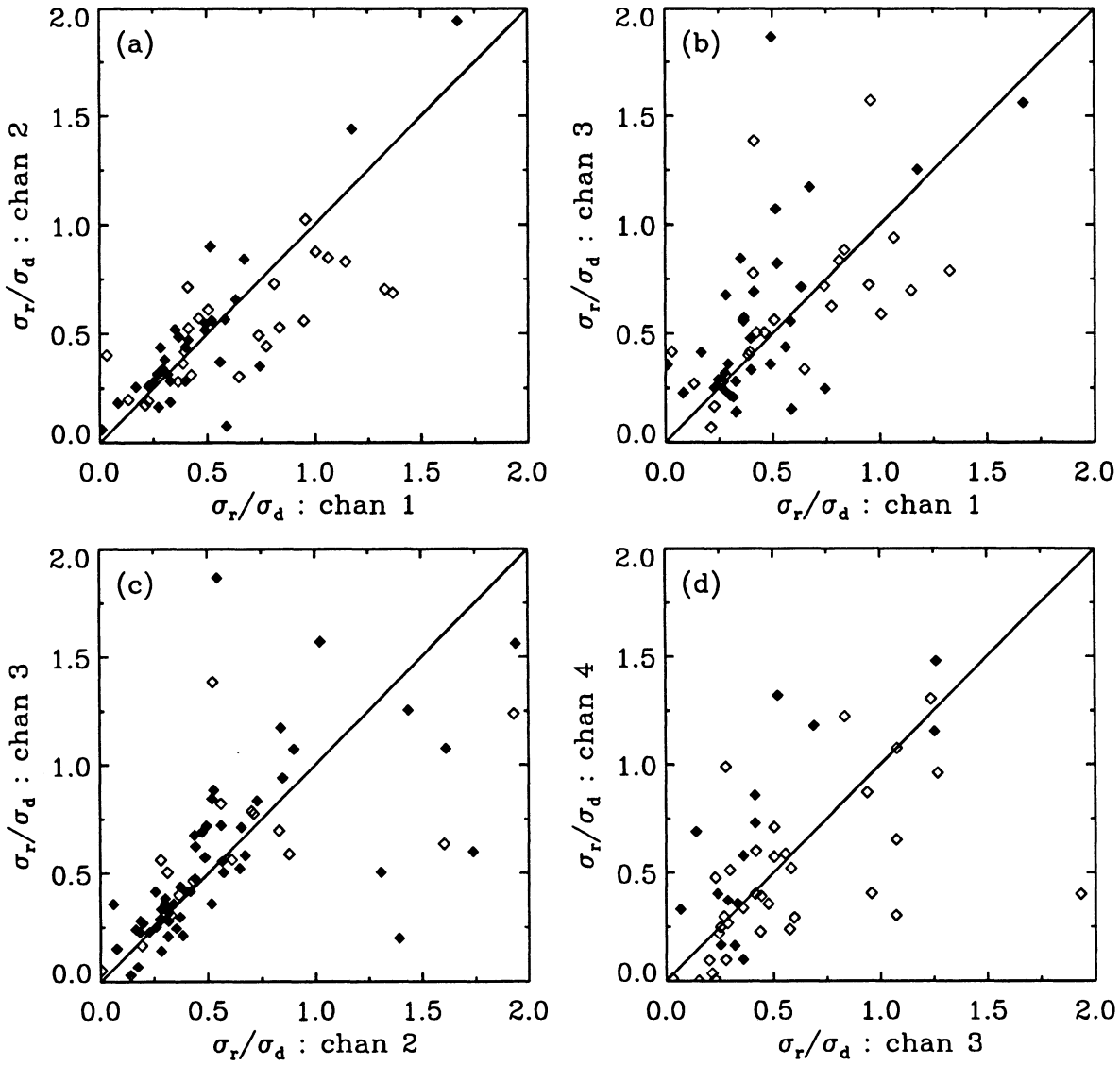

FIG. 8.—Similar to Fig. 7 for ratios of rise-to-decay parameters

Another illustration of self-similarity of pulse shape with energy is rise time versus decay time is plotted for channels 1 and 2 (Fig. 9*a*) and for channels 3 and 4 (Fig. 9*b*), for separable pulses. Channels 1 through 4 are indicated by squares, triangles, diamonds, and circles. Again, the more reliable determinations (for pulses with higher amplitudes) show a tighter correlation. Linear regressions for these points with filled symbols are indicated with dotted lines (channels 1 and 3) and dashed lines (channels 2 and 4). The fits are sufficiently similar that a single power-law relation serves for all four energy bands:

$$\sigma_r = 0.33\sigma_d^{0.83} . \quad (7)$$

The range in power-law index for the four channels, 0.80–0.85, is insignificant given the scatter in Figure 9. Then for our particular sample of bursts, the average σ_r/σ_d ratio ranges from 2.0 at $\sigma_d = 0.1$ s to 3.0 at $\sigma_d = 1.0$ s, essentially independent of energy. About three-fourths of all separable pulses fall within this range. Recall that the self-similarity relation of equation (6*b*), which requires $\sigma_r = C\sigma_d$, would apply for single pulses and therefore could still be consistent with the *trend for wider pulses to be more asymmetric* that equation (7) represents.

3.3. *Pulse Asymmetry, Width, and Hardness*

Now we examine connections between pulse asymmetry and various other derived parameters, such as pulse width, centroid lead/lag, and hardness ratio. First, Figure 10 illustrates for separable pulses the distributions of differences in times, between adjacent channels, of pulse peak and pulse centroid. The differences are indicated for channels 2-1 (*solid*), 3-2 (*dashed*), and 4-3 (*dotted*). The pulse centroid is the first moment in time of the counts distribution of the fitted pulse. A shift in pulse centroid necessarily includes any shift in pulse peak. There is a clear tendency for the peak in the higher channel to lead that in the lower channel (i.e., a negative ΔT) by an average of $\sim$20 ms, which translates into an average total of $\sim$60 ms lag in peak for channel 1 compared to channel 4. There is little difference in the peak lead/lag distributions. However, for pulse centroids, the largest average lag is obtained for channels 3-2 ($\sim$60 ms), with average lags of 25–30 ms for the other two differences, amounting to a cumulative average centroid lag, channels 4-1, of $\sim$120 ms. The average centroid shift is about one-third of the mode for pulse widths for separable pulses in channels 2 and 3 (Fig. 3*b*). The centroid distribution for channels 2-1 shows the longest tail toward positive

© American Astronomical Society • Provided by the NASA Astrophysics Data System

1996ApJ...459..393N

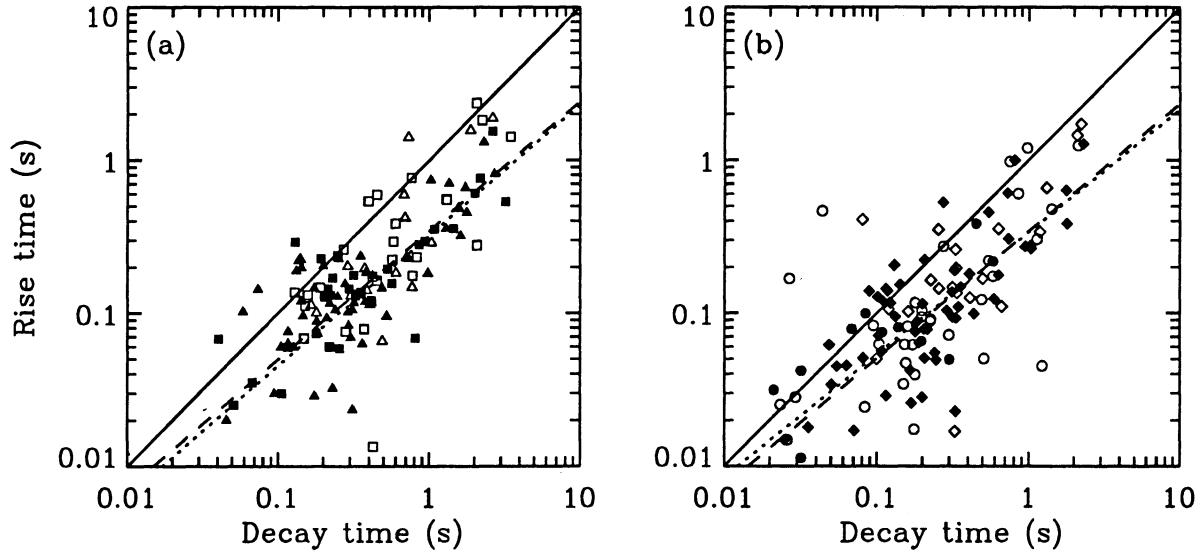

FIG. 9.—Plots of fitted rise vs. decay times, at 50% of pulse peak intensity. Symbols are (*a*) channels 1 (*squares*) and 2 (*triangles*), (*b*) channels 3 (*diamonds*) and 4 (*circles*). Filled and open symbols have same meaning as in Fig. 7. Linear regressions for filled symbols yield very similar fits in all four channels (*dots*, channels 1 and 3; *dashes*, channels 2 and 4). Over a range of approximately two decades, the average decay-to-rise ratio ranges from about 2 to 3, with large scatter, but essentially independent of energy.

values of ΔT, but this tail is probably spurious: Since pulses in channel 1 are the widest, have low statistics, and often have high values of v (tending to flat-topped pulses), we expect the least reliable determinations in peak and centroid lead/lag for channels 2-1. However, considerably longer tails in the centroid distribution extend to negative ΔT values of 300 ms.

Our result for average centroid lag between channels 4 and 1 of ~ 120 ms appears discrepant with a previous result. Much larger average lags ($\sim$factor of 3 higher) were determined for whole events, rather than for individual pulses, using cross Fourier analysis and a different set of bursts (Kouveliotou et al. 1992a). The discrepancy may be partly attributable to definitions: In the Fourier domain, average lags were computed across the range of frequencies required to represent whole events, including long tails of temporal structures. In the present analysis, we are considering only the difference in first moments of the pulse in two energy bands.

In Figures 11*a* and 11*b*, pulse asymmetry (σ_r/σ_d) is plotted versus the peak and centroid lead/lag, respectively. Filled and open symbols have the same meaning as in Figure 7 (similarly through Fig. 14), with the correspondence between channel and symbol shape as in Figure 9. In approximately 90% of pulses denoted with filled symbols (above amplitude threshold), lower energy lags higher energy and σ_r/σ_d is less than unity. Moreover, in Figure 11*b* the near-absence of pulses with high negative ΔT values *and* with σ_r/σ_d near unity signals the emergence of an interesting paradigm: As rise-to-decay ratio decreases from unity, resulting in a more asymmetric pulse, the pulse centroid is shifted to later times at lower energies. The significance of the trend between asymmetry and $\Delta T_{\rm centroid}$ was estimated by dividing the range in σ_r/σ_d into two subranges, at $\sigma_r/\sigma_d = 0.5$, and computing the means and sample errors under the assumption that the data are Gaussianly distributed. This is a zeroth-order approximation, and therefore the error estimates serve only as gross indicators of the real significances. Table 5A lists the average $\Delta T_{\rm centroid}$ and associated error for the two subranges. Since no dependence

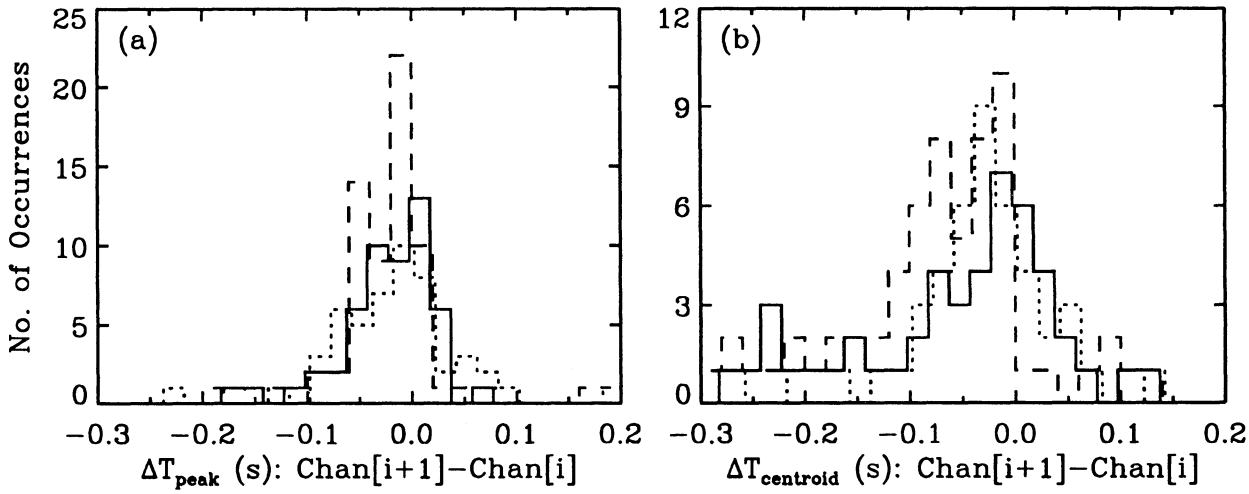

FIG. 10.—Distributions of differences in times between adjacent channels for (*a*) pulse peak and (*b*) pulse centroid, for separable pulses: channels 2-1 (*solid*), 3-2 (*dashed*), and 4-3 (*dotted*). The tendency is for the higher energy channel to lead the lower energy channel.

© American Astronomical Society • Provided by the NASA Astrophysics Data System

1996ApJ...459..393N

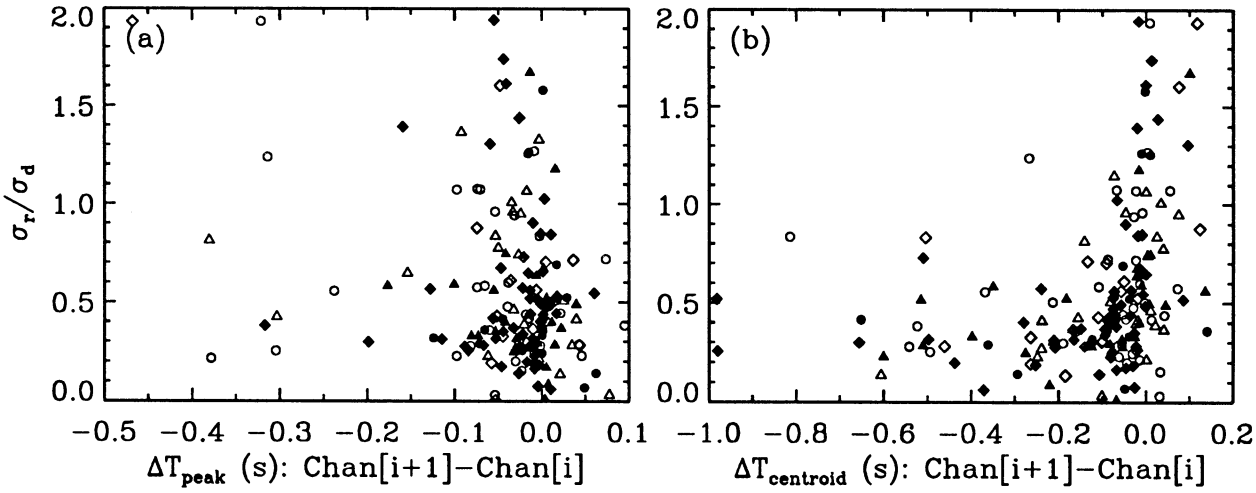

FIG. 11.—Pulse asymmetry (σ_r/σ_d) vs. differences in times between adjacent channels for (*a*) pulse peak and (*b*) pulse centroid for separable pulses. Filled and open symbols have the same meaning as in Fig. 7 (similarly through Fig. 14), with correspondence between channel and symbol shape as in Fig. 9. Approximately 90% of pulses denoted with filled symbols have negative ΔT and σ_r/σ_d less than unity.

TABLE 5

ESTIMATED SIGNIFICANCE OF TRENDS

A. PULSE ASYMMETRY VERSUS PEAK AND CENTROID LEAD/LAG[a]

Channel	Peak Amplitude Range (counts s^{-1})	Asymmetry Range	N_{pulse}	$\overline{\Delta T_{cen}}$ (ms)	ϵ_{cen} (ms)
1-2-3.....	>0.	$0.0 < \sigma_r/\sigma_d < 0.5$	106	162	+57, −17
		$0.5 < \sigma_r/\sigma_d < 2.0$	75	64	+44, −11
	>250.	$0.0 < \sigma_r/\sigma_d < 0.5$	63	198	+72, −25
		$0.5 < \sigma_r/\sigma_d < 2.0$	36	80	+192, −15

B. PULSE WIDTH VERSUS PEAK AND CENTROID LEAD/LAG[a]

Channel	Peak Amplitude Range (counts s^{-1})	FWHM Range(s)	N_{pulse}	$\overline{\Delta T_{cen}}$ (ms)	ϵ_{cen} (ms)
1.....	>0.	$0.1 < W < 0.6$	30	69	+60, −20
		$0.6 < W < 10.$	25	206	+64, −52
2.....	>0.	$0.1 < W < 0.5$	38	60	+12, −13
		$0.5 < W < 10.$	30	227	+94, −45
3.....	>0.	$0.1 < W < 0.4$	26	51	+14, −13
		$0.4 < W < 10.$	22	168	+116, −52

C. PULSE WIDTH VERSUS ASYMMETRY

Channel	Peak Amplitude Range (counts s^{-1})	FWHM Range(s)	N_{pulse}	$\overline{\sigma_r/\sigma_d}$	$\epsilon_{\sigma r/\sigma d}$
1-2.....	>0.	$0.1 < W < 0.4$	46	0.67	+0.24, −0.07
		$0.4 < W < 10.$	78	0.51	+0.10, −0.03
	>250.	$0.1 < W < 0.4$	36	0.66	+0.34, −0.07
		$0.4 < W < 10.$	42	0.45	+0.13, −0.03
3-4.....	>0.	$0.1 < W < 0.25$	12	0.83	+0.16, −0.11
		$0.25 < W < 10.$	44	0.73	+0.22, −0.07
	>250.	$0.1 < W < 0.25$	8	0.90	+0.16, −0.19
		$0.25 < W < 10.$	8	0.43	+0.42, −0.04

D. HARDNESS RATIO VERSUS CENTROID LEAD/LAG[a]

Channel	Peak Amplitude Range (counts s^{-1})	Hardness Ratio Range	N_{pulse}	$\overline{\Delta T_{cen(3-2)}}$ (ms)	ϵ_{cen} (ms)
3/2.....	>0.	$0.0 < HR_{3/2} < 1.25$	57	161	+73, −23
		$1.25 < HR_{3/2} < 2.50$	15	20	+10, −43

[a] Positive values signifies lower energy lags higher energy

© American Astronomical Society • Provided by the NASA Astrophysics Data System

1996ApJ...459..393N

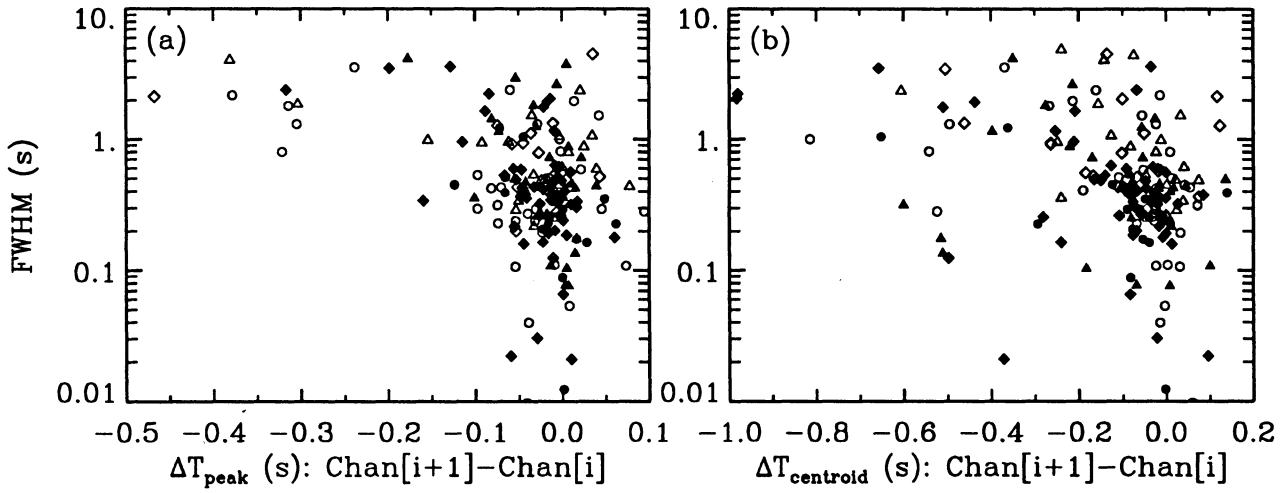

FIG. 12.—Pulse width vs. differences in times between adjacent channels for (*a*) pulse peak and (*b*) pulse centroid for separable pulses. Same symbol meanings as in Fig. 11.

of pulse asymmetry on energy was found (eq. [7]), and since the distribution for $\Delta T_{\rm centroid}$ is approximately independent of energy (Fig. 10), all points in Figure 11*b* were included in the averaging procedure. For conciseness in the table, positive ΔT indicates that low energy leads high energy (opposite to the sense in Fig. 10). Very different positive and negative (usually smaller) error bars are an indication of the non-Gaussian distribution of data points. The difference in $\Delta T_{\rm centroid}$ between the subranges in σ_r/σ_d is formally significant at slightly more than the 2 σ level. Using only pulses with peak amplitudes above the amplitude threshold (*filled symbols*) yields comparable averages for $\Delta T_{\rm centroid}$, but the difference between subranges is then not significant.

In Figures 12*a* and 12*b* pulse width is plotted versus peak and centroid lead/lag, respectively. Here we see a tendency for wider pulses to exhibit longer lags. This relationship might be expected since the major part of the lag results from a shift in centroid rather than time of peak, and therefore longer pulses will have centroids further shifted than will short pulses as the pulse narrows toward higher energy. Because pulse width narrows with energy, we estimated the significance of this trend separately for pulse widths in channels 1–3, adjusting the division in width range to yield approximately equal numbers of pulses in the respective subranges. Results are shown in Table 5B. For each channel, the differences in average $\Delta T_{\rm centroid}$ for the width subranges have formal significances of 2.3, 3.7, and 2.2 σ for channels 1–3, respectively. Again, utilizing all pulses in Figure 12 (no amplitude threshold) yields the most significant results.

The connection between pulse width and asymmetry is made in Figure 13. Figure 13*a* shows the relationship for channels 1 and 2. Again, considering higher amplitude pulses (*filled symbols*), the appearance of fewer wide pulses with σ_r/σ_d near unity extends the paradigm: wider pulses tend to be more asymmetric. This trend is not as clearly defined, but still is present in Figure 13*b*, which shows channels 3 and 4; the poorer definition might arise, as suggested for the two higher energy channels in Figures 7 and 8, from narrower pulses and fewer points with which to define the pulse shape (σ_r/σ_d). A similar procedure was followed to estimate the significance of the apparent trend, dividing the width range into subranges such that approximately equal numbers of pulses were obtained for those pulses above the amplitude threshold. Channels 1 and 2 and channel 3 and 4 were combined to increase statistics. Only the former com-

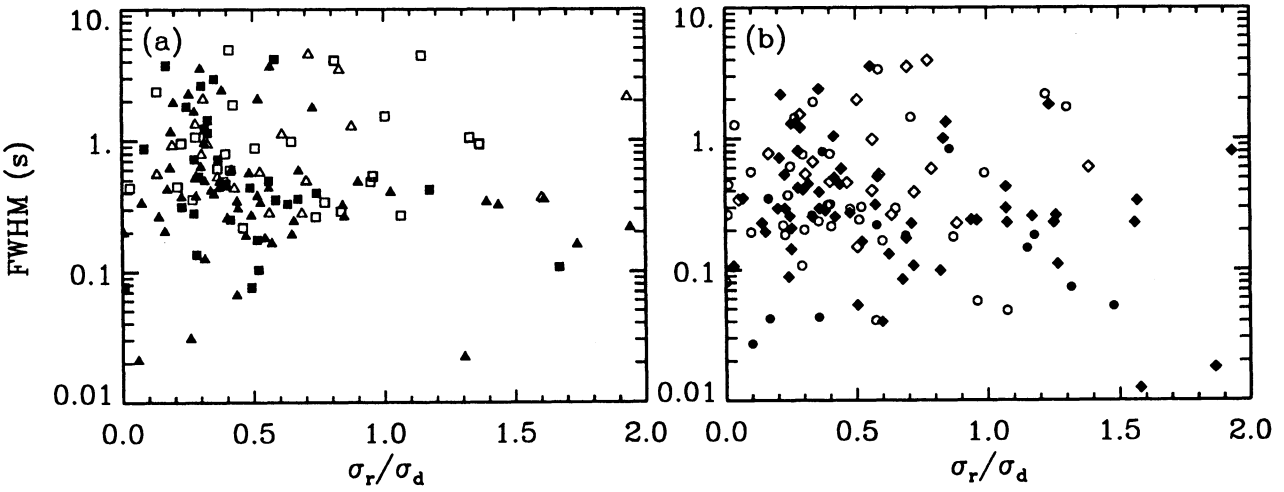

FIG. 13.—Pulse width vs. asymmetry for separable pulses. (*a*) Channels 1 and 2; (*b*) channels 3 and 4. Same symbol meaning as in Fig. 11.

© American Astronomical Society • Provided by the NASA Astrophysics Data System

1996ApJ...459..393N

bination yields a significant difference, at the 2–2.5 σ level, in average asymmetry between the two width subranges (Table 5C).

Now we investigate how this paradigm might be related to pulse spectral hardness. Since channels 3 and 2 routinely have the most counts, we define an integral spectral hardness, $HR_{3/2}$, as the ratio of total counts within the fitted pulses for these two channels. (Similar results, not shown, are found for the hardness ratios $HR_{2/1}$ and $HR_{4/3}$.) Figure 14 illustrates $HR_{3/2}$ plotted versus pulse centroid lead/lag for (*a*) channels 3-2 and (*b*) versus pulse asymmetry, (*c*) width, and (*d*) rise time in channel 2. The lead/lag plot shows a possible trend, with a subpopulation of hard pulses at $\Delta T_{centroid}$ near zero lag. Utilizing all points in Figure 14*a*, and dividing the hardness ratio range in half, we find a significant difference in average $\Delta T_{centroid}$ for the two subranges (Table 5D). From the relationships between pulse width, asymmetry, and centroid lead/lag in Figures 11–13, we would expect related trends in Figure 14. Even considering only the filled symbols designating higher amplitude pulses, there is only a slight trend for narrower, more symmetric pulses to be spectrally harder. Also, there is only a slight indication of the trend reported by Kouveliotou et al. (1992b) for pulses with shorter rise times to be harder. However, that relationship was found for single-pulse events. Since our sample contains mostly many-pulse events, we expect that, since bursts often soften as they progress, thus producing softer pulses later, correlations between pulse spectral hardness and shape may be diluted.

4. DISCUSSION

From a phenomenological point of view, it has not been clear what the fundamental "event" is in gamma-ray bursts, that is, whether bursts are composed of pulses, or noise processes on a continuum of timescales, or both. The results presented here shed some light on this problem for a wide variety of burst profiles. Our working premise has been that pulses are the basic unit in bursts. We find several mutually reinforcing trends which support this hypothesis.

First, most fitted pulses exhibit the familiar softening trend that has been widely observed for conglomerate pulse structures, an indication that the primary energy generation mechanism is manifested and temporally resolved on the pulse timescale. Second, the pulse model we employ usually results in a parsimonious representation of burst profiles in that a relatively small number of pulses is required to achieve an acceptable fit. However, there is a tendency for tall spiky pulses seen in the higher channels to be subsumed into wider, smoother structures in channel 1, to the extent that, had there not been a definitive indication of existence at high energy, the pulse peak at low energy would have been apprehended to be merely a statistical fluctuation.

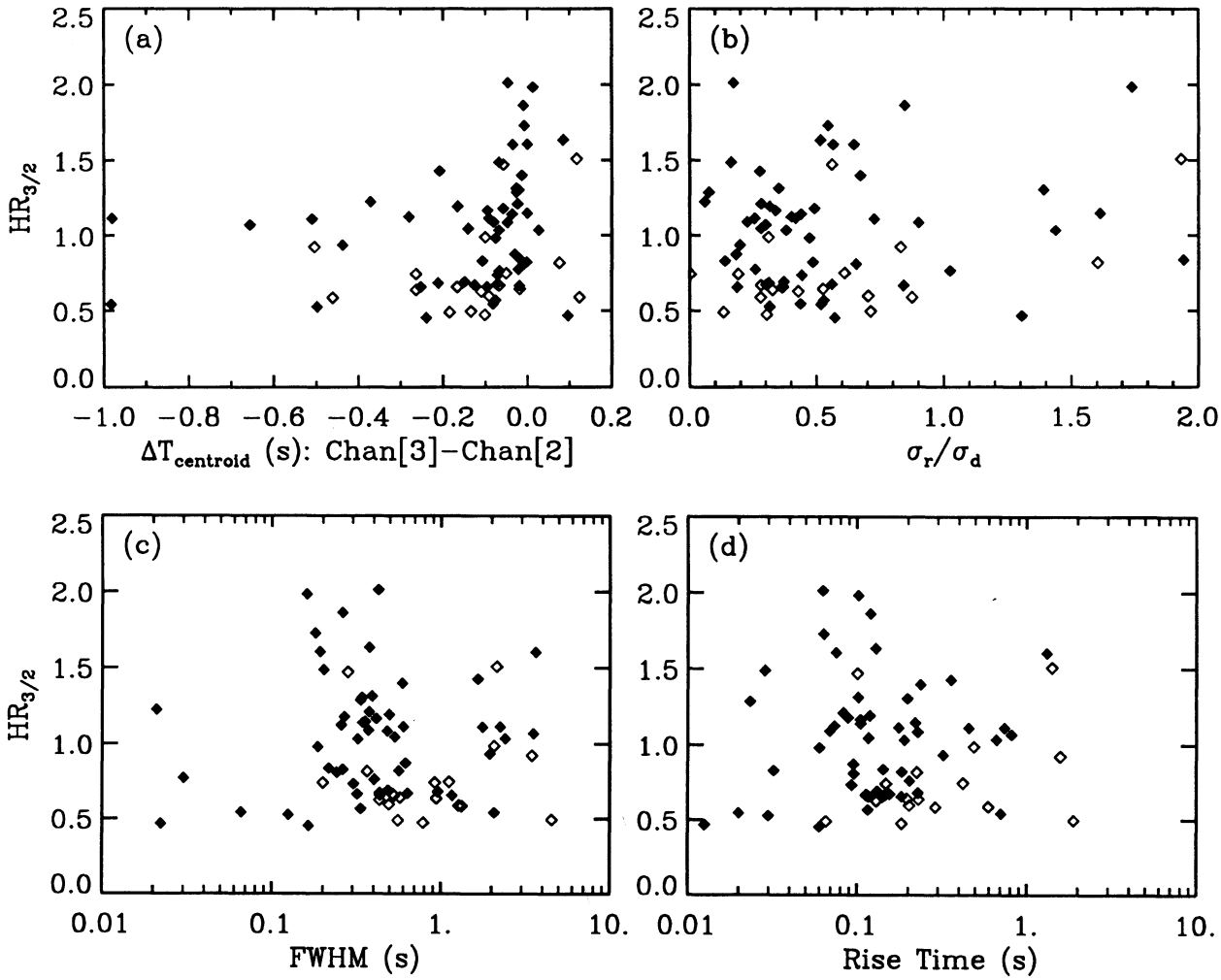

FIG. 14.—(*a*) Pulse hardness ratio, channels 3:2 ($HR_{3/2}$), vs. pulse centroid lead/lag for same channels for separable pulses. Similarly, $HR_{3/2}$ vs. (*b*) pulse asymmetry, (*c*) width, and (*d*) rise time in channel 2.

© American Astronomical Society • Provided by the NASA Astrophysics Data System

1996ApJ...459..393N

Notwithstanding this observation, there may be other components in bursts, undefined by our approach, including long smooth structures at lower energies and very short spiky features at higher energies, which might represent physical processes distinct from the pulse process. Evidence for this possibility in at least some bursts comes from those five which we were not successful at fitting with pulses. In each case, especially in channel 1, the visual appearance suggests that in some regions, pulses were superposed on top of a broader, smooth component. These broad components could in principle be fitted with our pulse model, but the least-squares algorithm invariably would fail as a result of matrix inversion problems, probably exacerbated by the large number of pulses declared to be present.

Several other compelling trends reinforce the reality of the pulse component. When we select samples of fitted pulses on the basis of separability—total and separable samples—we find the average pulse profiles to be very similar but slightly broader for the total sample. The ratio of pulse widths as a function of energy is very similar for the two samples, and the modes for their pulse peakedness distributions are comparable. Differences between the two samples appear attributable mostly to the difficulties of deconvolution of overlapping pulses. There is a clear trend as a function of energy for pulse shape to be self-similar: rise-to-decay ratio and pulse peakedness for well-determined pulses (above an amplitude threshold), are comparable in the four energy channels. Approximate self-similarity is evidence of organization as a function of energy. Moreover, this organization extends over a range of a factor of 100 in pulse width, such that the average rise-to-decay ratio changes only slowly from ~ 2 to 3, essentially independent of energy. In addition, the form of pulse width dependence on energy is approximately power law (see Fenimore et al. 1995), with an index of ~ -0.40 over the energy range ~ 25 keV–1 MeV.

We find important connections between pulse asymmetry, width, and spectral softening: Among pulses for which shape is relatively well determined, the rise-to-decay ratio is usually unity or less; as this ratio decreases, pulses tend to be wider, and the pulse centroid is more shifted to later times at lower energies. We conjecture that pulses with reversed-FRED shape—exponential rise, fast decay (ERFDs)—are rare or do not exist. Given that most pulses overlap substantially, the $\sim 10\%$ of separable pulses above the amplitude threshold which appear as ERFDs could easily be accounted for as superpositions of FREDs. Similarly, the $\sim 10\%$ of these pulses for which the pulse centroid leads (only slightly) at low energy may be explained by such superpositions or by statistical fluctuations.

Therefore, we propose the asymmetry/width/softening connection as a general pulse paradigm in gamma-ray bursts. This is illustrated schematically in Figure 15. From studying the fits of pulses in a relatively small sample (12) of short bursts (Norris et al. 1993), we suspect that the paradigm continues on shorter timescales, but this suspicion needs to be quantified in terms of self-similarity: Can a scaling factor be applied to short bursts such that Figure 15 is reproduced? If so, then we are led to some speculations. First, the pulse paradigm would be another unifying principle between short and long bursts, in addition to the commonality of isotropic celestial distributions and comparable ranges in peak intensity (Fishman et al. 1994). Second, note that pulse widths in short bursts cluster in the tens of milliseconds (Norris et al. 1993), whereas for long bursts the mode is in the hundreds of milliseconds, only an order of magnitude longer. The entire range of pulse widths is ~ 10 ms–2 s, a factor of ~ 200. In comparison, durations range over 5 orders of magnitude, ~ 10 ms–1000 s. Thus explaining temporal variability in pulses, which we take to be the basic units of emission in bursts, is relatively less difficult than explaining burst durations.

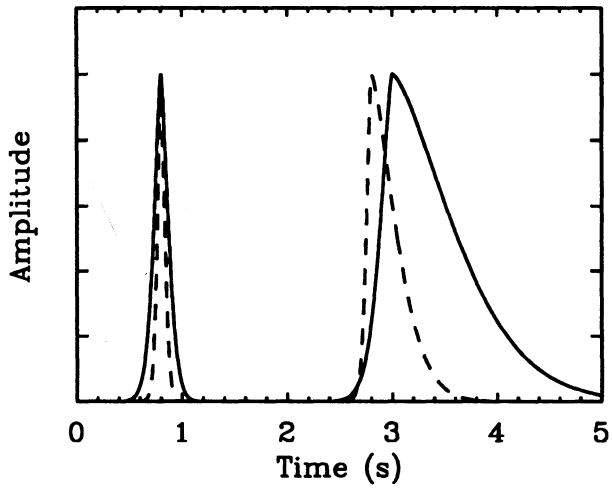

FIG. 15.—Proposed pulse asymmetry/energy-shift paradigm: *Solid curve:* low-energy (few × 10 keV) emission; *dashed curve:* high-energy (few × 100 keV) emission. Pulse shapes range from narrow and symmetric with negligible centroid shift with energy, to wide and asymmetric with centroid shift comparable to FWHM. A portion (less than half) of centroid shift is accounted for by shift in time of pulse maximum; balance arises from widening of pulse at lower energies. Extent of widths and asymmetry illustrated here represents range of behavior for most pulses in separable sample (see Fig. 13).

We can conjecture that the range in pulse width might be divisible into two cofactors, one which accounts for the variation in asymmetry, associated with a variation of a factor of ~ 10 in pulse width, and another factor of comparable magnitude which scales short pulses in short bursts into long pulses in long bursts. The asymmetry factor could conceivably arise from differences in perceived geometry, such as viewing angle. In fact, since a range in pulse asymmetry is apparent even when only the initial temporal structures in bursts are considered, scenarios involving perfectly spherical beaming with no interaction with the surrounding environment would seem not to be favored. The remaining factor in pulse width, which would scale short pulses to long ones, might then be identified with a bulk relativistic beaming factor (see Baring 1994 for review of burst scenarios). This is consistent with the observation that short bursts are, on average, spectrally harder than long bursts (Kouveliotou et al. 1993) and with the slight trend we identify for more symmetric, narrower pulses to be harder. The observed spectral hardness of a pulse, however, would also be a function of intrinsic beaming factor and position within a burst (for unknown physical reasons), since bursts often soften as they progress (Norris et al. 1987; Ford et al. 1995). In addition, an inverse correlation between pulse structure hardnesses and time between pulses has been identified in *PVO* bursts (Lochner 1992). It is clear that clarifications of spectral dependencies and their relationships to temporal aspects are necessary to verify and extend our conjecture pulse paradigm.

There are two other important questions regarding the pulse paradigm to be pursued. First, do entire bursts tend to

© American Astronomical Society • Provided by the NASA Astrophysics Data System

1996ApJ...459..393N

obey the correlations between pulse asymmetry, width, and softening? Two examples of bursts with many narrow, symmetric pulses are trigger numbers 678 and 1606, illustrated in Nemiroff et al. (1994), and two examples of bursts with a few, wide, asymmetric pulses are trigger numbers 543 and 1085 (see first BATSE catalog, Fishman et al. 1994). Many other such examples are apparent. Although it may be a general trend for pulses in bursts to be mostly symmetric or mostly asymmetric, a quantitative investigation of all bursts is needed to determine how closely this picture is obeyed or to what degree it is violated. Second, are pulses really symmetric in the limit, or is the finding of symmetry limited by the temporal resolution employed? In fact, on the shortest timescales we have examined (down to 16 ms) in trigger number 678, the test for asymmetry described in Nemiroff et al. finds negligible asymmetry; this burst is marginally asymmetric only on timescales longer than 4 s, much longer than the timescales of its narrow constituent pulses. Better determinations might employ "time-to-spill" data, for which resolution increases as the counting rate increases.

We conclude from the distribution of intervals between pulses, which exhibits a broad maximum near 1 s, that there is a "characteristic timescale" between pulses, previously noted by other investigators (Desai 1981). This finite mode (a mode of zero with exponentially decreasing distribution is expected for random placement) and the propensity for short bursts (Norris et al. 1994b) to have few, closely spaced pulses may account naturally for the bimodal duration distribution (Kouveliotou et al. 1993). Firmer support for this conjecture awaits analysis of a larger sample of bursts near the minimum between the two modes.

These results have been obtained using a pulse model that perhaps allows for more degrees of freedom (five) than ultimately required (but nonetheless necessary in order to explore a sufficiently liberal parameter space), given that the sample of separable pulses shows a remarkable tendency toward pulses with rise-to-decay ratios less than unity. Thus, we expect that viable physical models would probably reduce the number of shape parameters from three to two in some manner which connects the rise and decay portions (for instance, a log-normal pulse; Brock et al. 1994).

APPENDIX

We wish to convey an appreciation of the degree of success and difficulty encountered in the process of fitting pulses to gamma-ray bursts. This is best achieved by illustrating the fits themselves for a representative subset of the 41 bursts analyzed in this work. The fits shown in Figures 16–25 fairly closely reflect three important, related aspects of the total sample: distribution in reduced χ^2, range of burst appearance, and degree of pulse overlap or separation. Each figure consists of four panels corresponding to the four energy bands, with channel 1 at top. Extent on the time axis ranges from $\sim$10 s to 64 s. Intensity is plotted in counts per bin. Fitted pulses are indicated at the top of each panel and numbered per channel. Different numbers of pulses are usually fitted in the several channels, for which the ordinal pulse numbering is not necessarily in correspondence. The total model is shown with a narrow solid line, either above or coincident with individual pulses, which are shown with slightly wider lines. The bursts are arranged approximately in order of increasing complexity.

Often, the fit for channel 3 has the highest χ^2; this is related to the fact that, for bright bursts, channel 3 almost always has

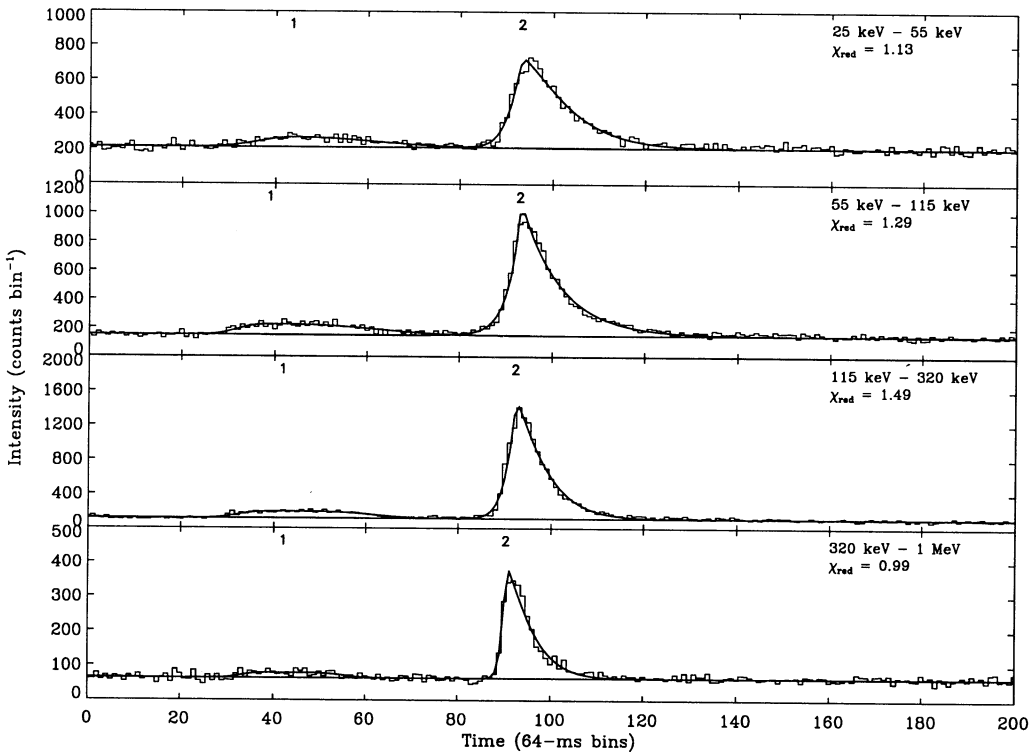

FIG. 16.—BATSE trigger 999: a simple burst profile, with two fitted pulses. Both pulses, identified in all four channels, are considered separable since their overlap is insignificant.

© American Astronomical Society • Provided by the NASA Astrophysics Data System

1996ApJ...459..393N

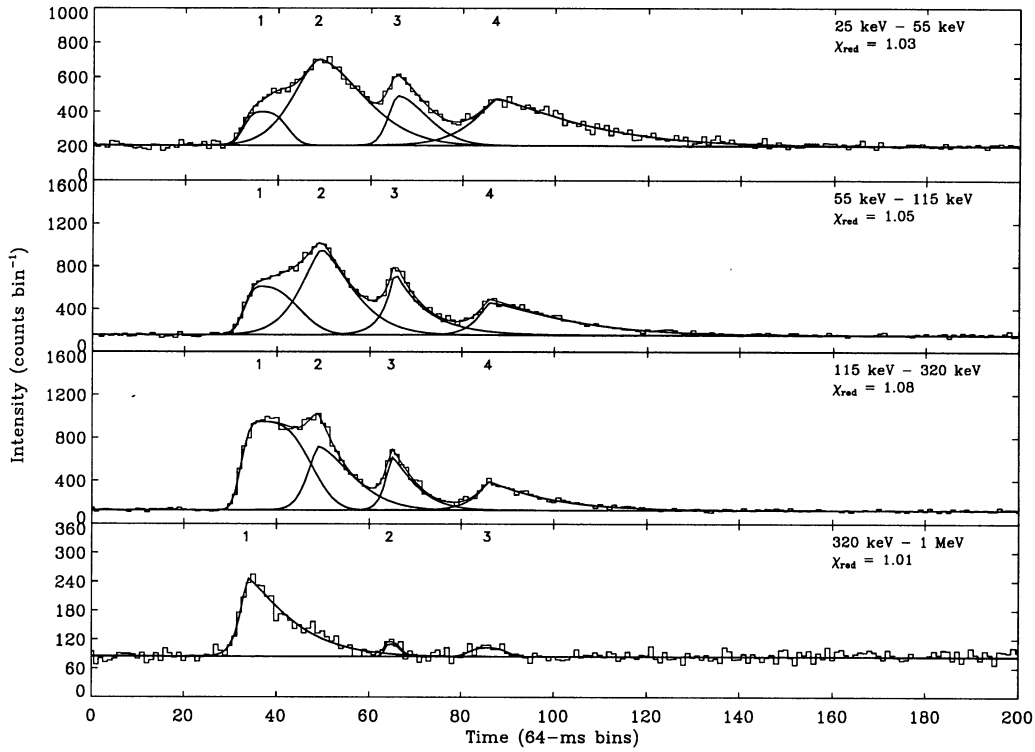

FIG. 17.—BATSE trigger 543. Four pulses are required to fit profiles in channels 1–3, whereas a second pulse is not required in channel 4. Pulse no. 4 in channels 1–3 and pulse no. 3 in channel 4 are separable pulses. Pulses no. 3 (channel 3) and no. 2 (channel 4) are also separable.

the highest count rate. Thus, whereas the sum of fitted pulses will represent fairly well the total emission, the actual temporal profile may contain "hidden" pulses which were not specified and which therefore contribute significantly to χ^2 in an intense burst. Since such pulses severely overlap their neighbors, they are by definition not "separable" and are not included in our analyses which relate information in more than one channel. An alternative explanation for poor fits is that our pulse model is not sufficiently detailed to represent the individual emission events when they are defined with very good statistics.

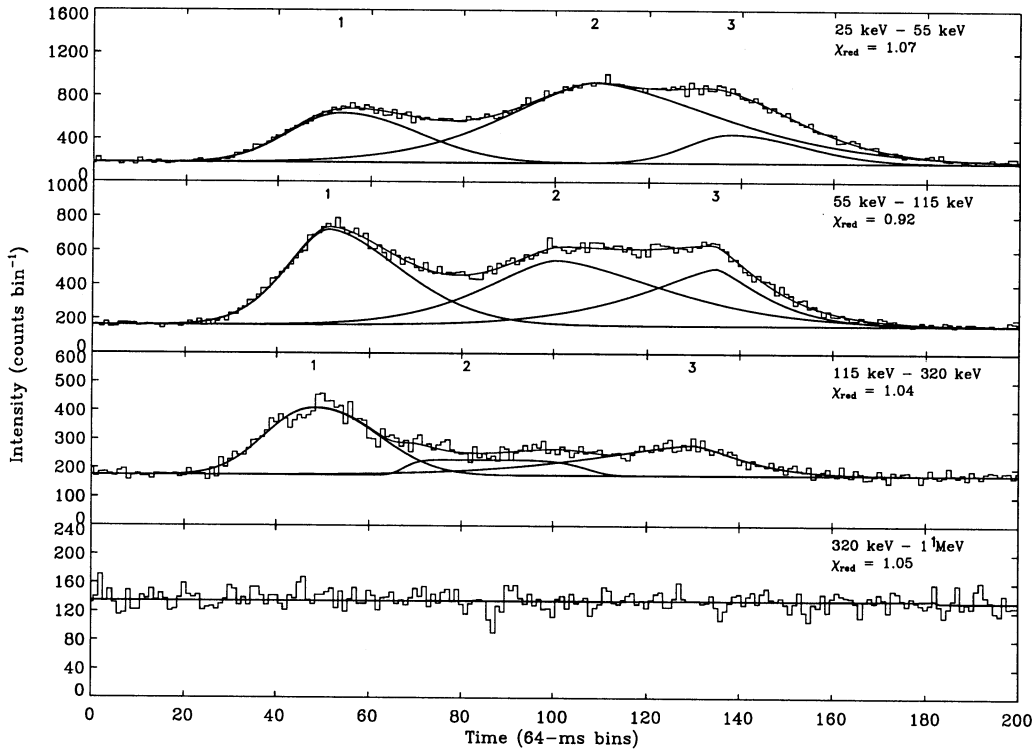

FIG. 18.—BATSE trigger 1974: three relatively wide pulses are required for a good fit; none are separable

© American Astronomical Society • Provided by the NASA Astrophysics Data System

1996ApJ...459..393N

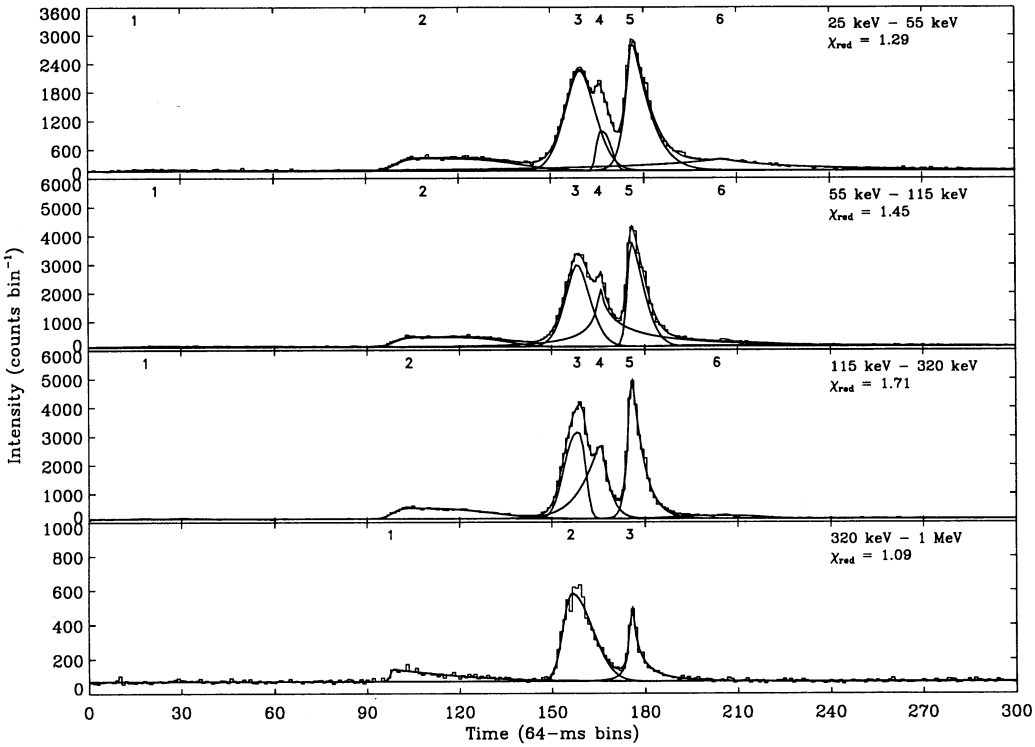

FIG. 19.—BATSE trigger 1609, pulse no. 4, channel 2, exemplifies a ubiquitous problem: the wings of a "sandwiched" pulse intrude into the domain of adjacent pulses. Similarly, the low-intensity pulse no. 6, channel 1, extends backward across four pulses. Reduced χ^2 for channel 3 is relatively high, reflecting a well-determined light curve.

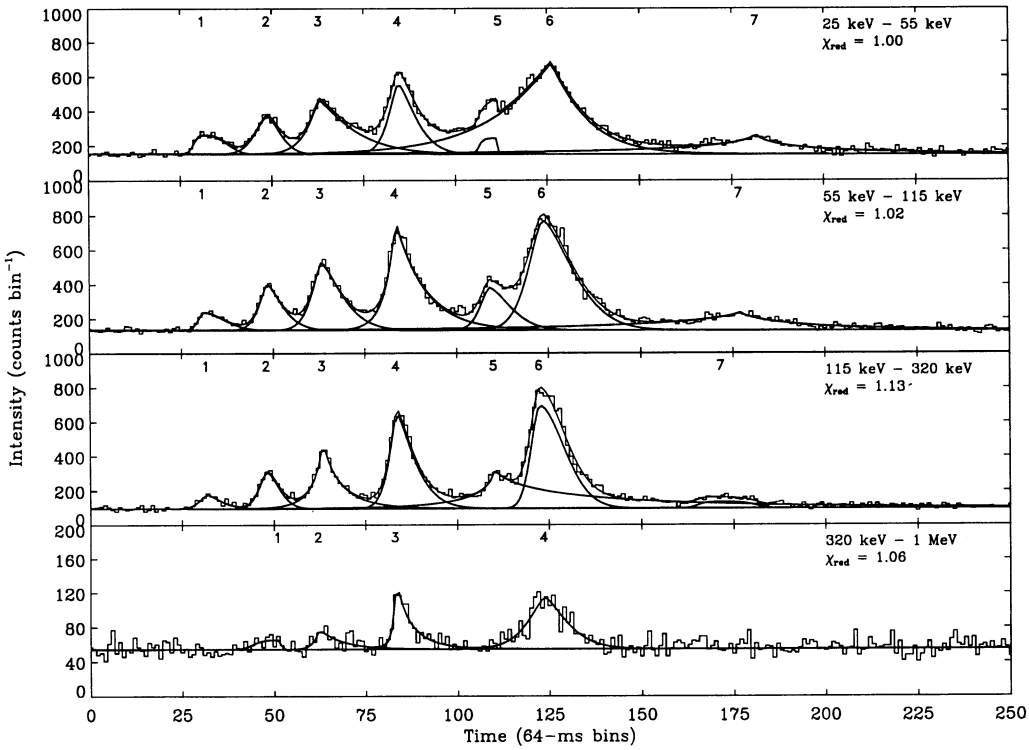

FIG. 20.—Seven major pulses apparent in channels 1–3 of BATSE trigger 1425, but a low counting rate permits identification of only four pulses in channel 4.

© American Astronomical Society • Provided by the NASA Astrophysics Data System

1996ApJ...459..393N

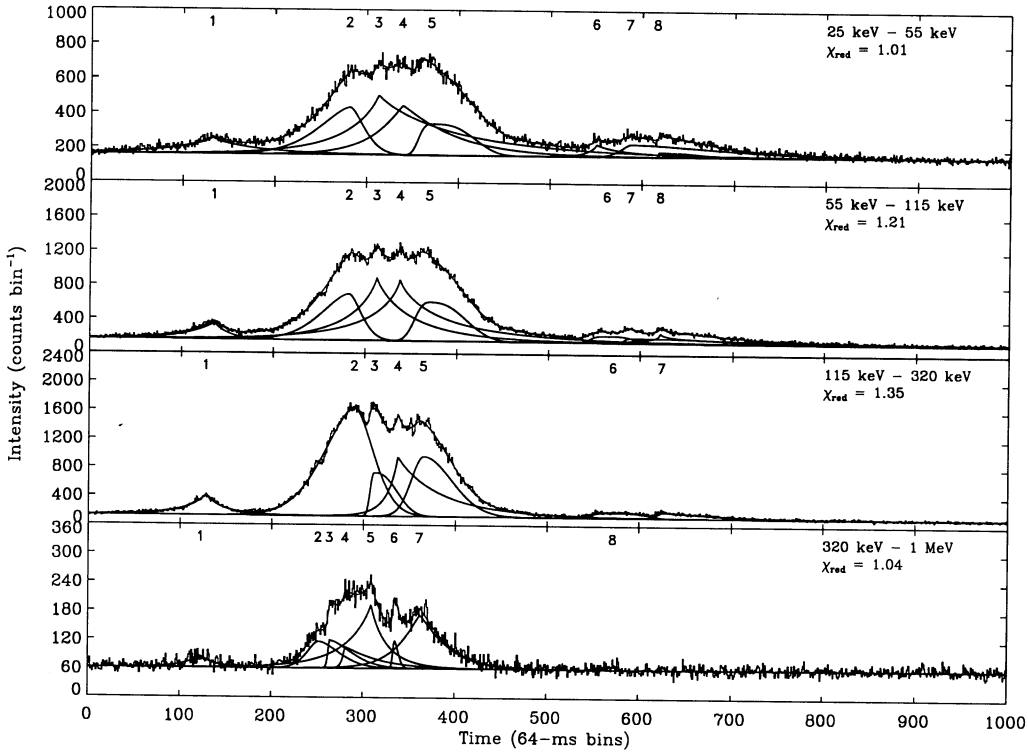

FIG. 21.—BATSE trigger 2067 has a relatively smooth major pulse structure which nevertheless requires several pulses to fit the individual, blended peaks

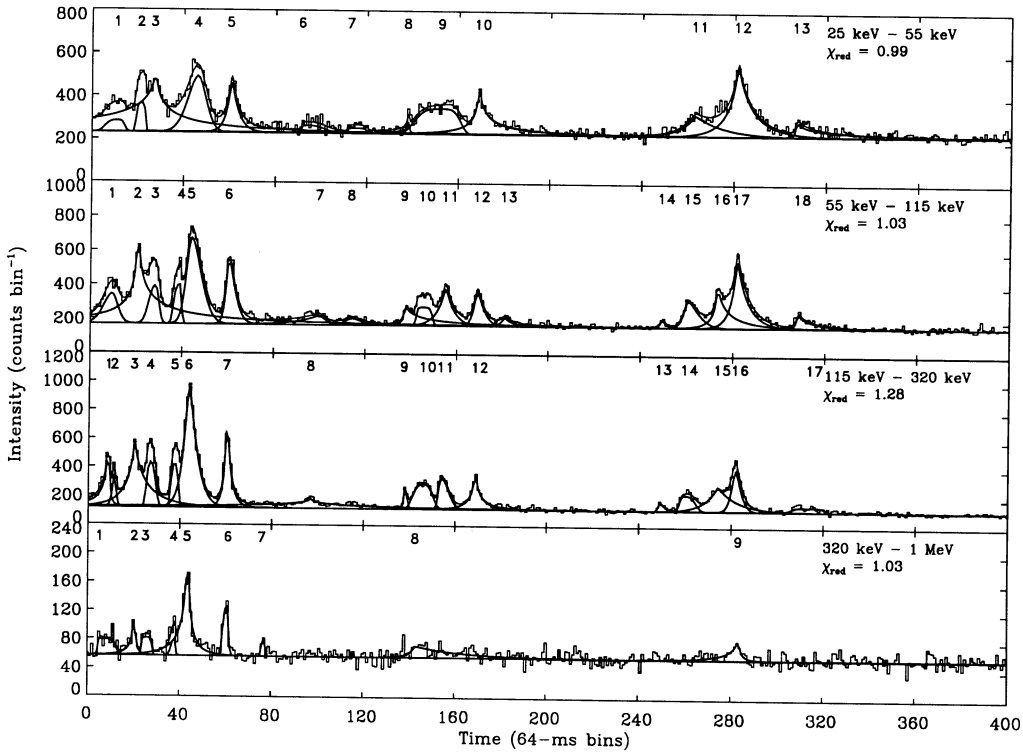

FIG. 22.—BATSE trigger 2228 is a long burst with many pulses, but only a few separable ones. In channel 4, only half the number of pulses appear as in channels 2 and 3.

© American Astronomical Society • Provided by the NASA Astrophysics Data System

1996ApJ...459..393N

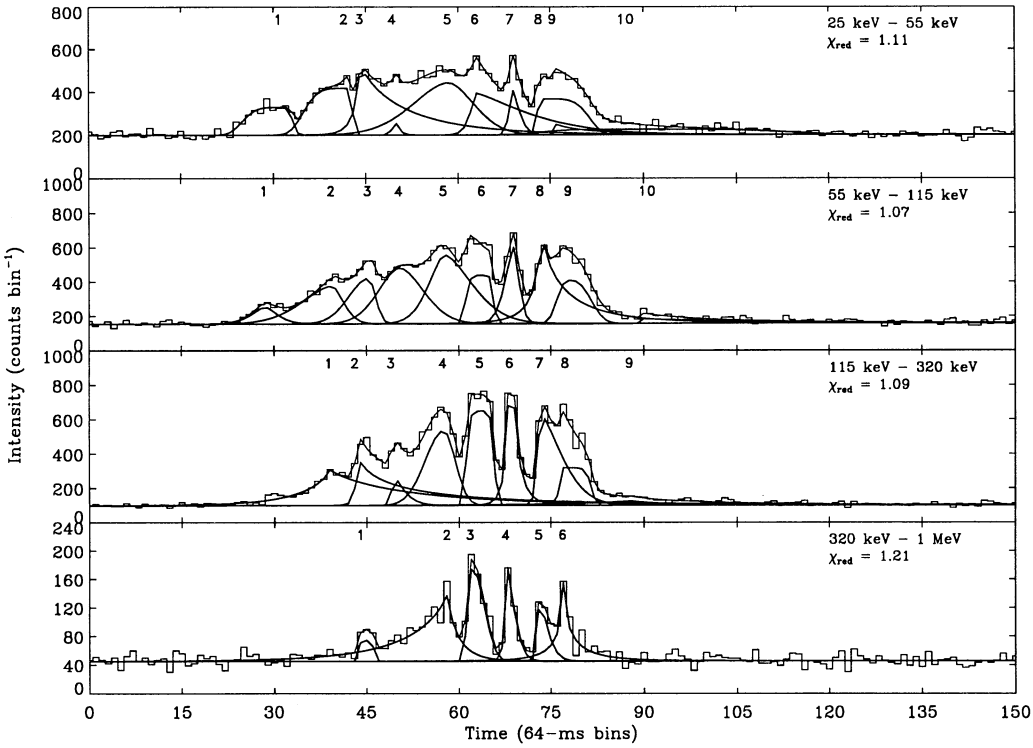

FIG. 23.—BATSE trigger 1683 is an example of a burst with several pulses in which the overlapping is acute at lower energies

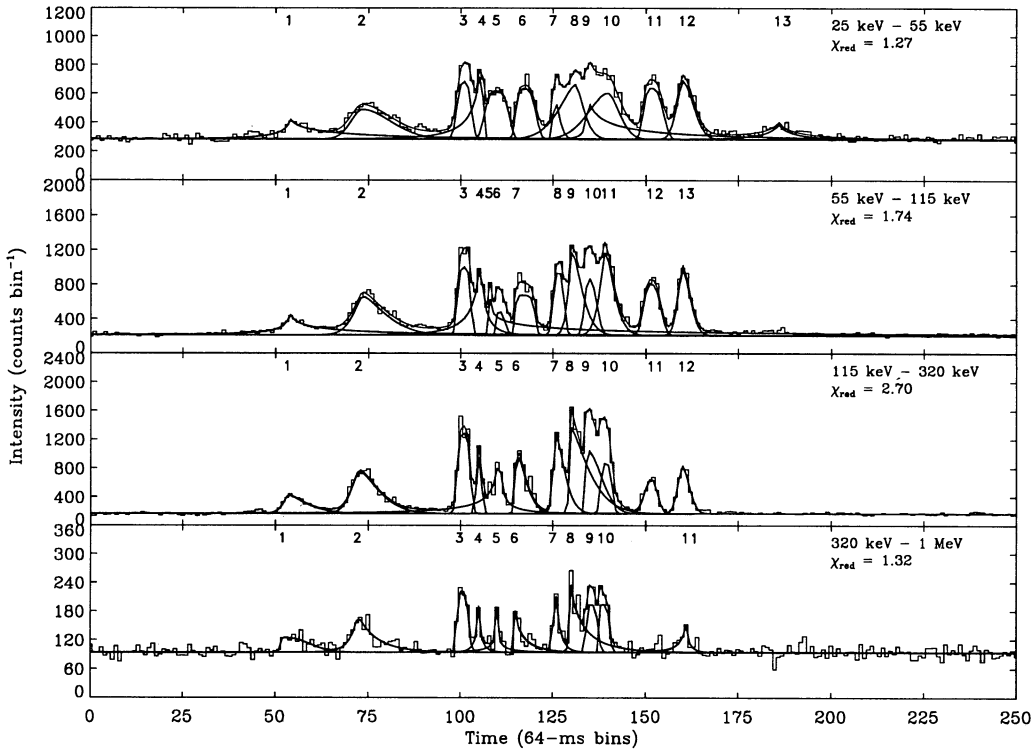

FIG. 24.—BATSE trigger 1440 is a many-pulsed burst, with several examples of wings of interior pulses intruding past several neighboring pulses. It is apparent that unambiguous pulse fits require more than just distinct peaks; pulses must be sufficiently separated to better define rise and decay.

© American Astronomical Society • Provided by the NASA Astrophysics Data System

1996ApJ...459..393N

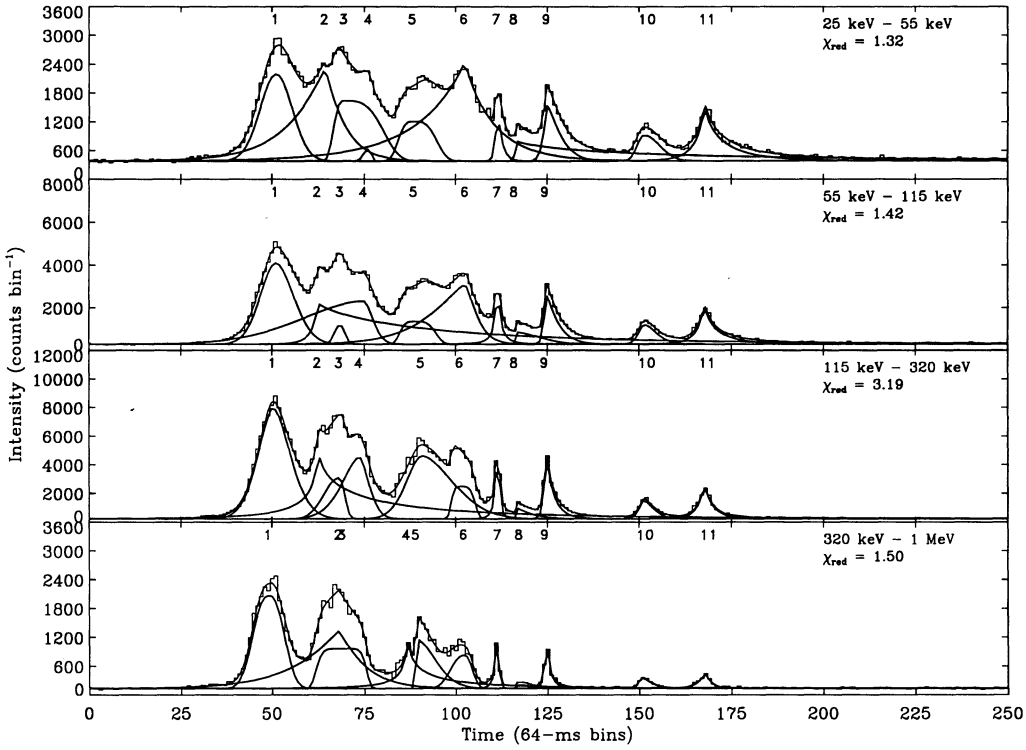

FIG. 25.—First outburst of the famous 1991 May 3 event, BATSE trigger 143. First, second, and third major pulse structures are not well fitted (although six pulses were specified in the attempt), as reflected in the poor reduced χ^2 statistics.

REFERENCES

Baring, M. G. 1994, in Currents in High Energy Astrophysics, ed. J. Wefel, R. Silberberg, & M. Shapiro (Dordrecht: Kluwer), 21
Brock, M., et al. 1994, in AIP Conf. Proc. 307, Gamma-Ray Bursts, ed. G. J. Fishman, J. J. Brainerd, & K. Hurley (New York: AIP), 672
Davis, S. P., Norris, J. P., Kouveliotou, C., Fishman, G. J., Meegan, C. A., & Paciesas, W. S. 1994, in AIP Conf. Proc. 307, Gamma-Ray Bursts, ed. G. J. Fishman, J. J. Brainerd, & K. Hurley (New York: AIP), 182
Desai, U. D. 1981, Ap. Space Sci., 75, 15
Fenimore, E. E., & Bloom, J. S. 1995, ApJ, 453, 25
Fenimore, E. E., In't Zand, J. J. M., Norris, J. P., Bonnell, J. T., & Nemiroff, R. I. 1995, ApJ, 448, L101
Fishman, G. J., et al. 1989, in Proc. Gamma Ray Observatory Science Workshop, ed. W. N. Johnson (Greenbelt: NASA/GSFC), 2–39
Fishman, G. J., et al. 1994, ApJS, 92, 229
Ford, L. A., et al. 1995, ApJ, 439, 307
Hurley, K. 1991, in AIP Conf. Proc. 265, Gamma-Ray Bursts, ed. W. S. Paciesas & G. J. Fishman (New York: AIP), 3
Kouveliotou, C., et al. 1992a, in AIP Conf. Proc. 265, Gamma-Ray Bursts, ed. W. S. Paciesas & G. J. Fishman (New York: AIP), 299
———. 1992b, in The Compton Observatory Science Workshop, ed. C. R. Shrader, N. Gehrels, & B. Dennis (Greenbelt: NASA/GSFC), 61
Kouveliotou, C., Meegan, C. A., Fishman, G. J., Bhat, N. P., Briggs, M. S., Koshut, T. M., Paciesas, W. S., & Pendleton, G. N. 1993, ApJ, 413, L101
Link, B., Epstein, R. I., & Priedhorsky, W. C. 1993, ApJ, 408, L81
Lochner, J. C. 1992, in AIP Conf. Proc. 265, Gamma-Ray Bursts, ed. W. S. Paciesas & G. J. Fishman (New York: AIP), 289
Nemiroff, R. J., et al. 1993, ApJ, 414, 36
———. 1994, ApJ, 423, 432
Norris, J. P. 1983, Ph.D. dissertation, Univ. Maryland
Norris, J. P., Kouveliotou, C., Fishman, G. J., Meegan, C. A., Paciesas, W. S., & Wilson, R. B. 1992, in AIP Conf. Proc. 265, Gamma-Ray Bursts, ed. W. S. Paciesas & G. J. Fishman (New York: AIP), 294
Norris, J. P., et al. 1986, ApJ, 301, 213
———. 1987, Adv. Space Res., 6, 19
———. 1993, in AIP Conf. Proc. 280, Compton Gamma-Ray Observatory, ed. M. Friedlander, N. Gehrels, & D. J. Macomb (New York: AIP), 959
Norris, J. P., et al. 1994a, ApJ, 424, 540
Norris, J. P., Nemiroff, R. J., Davis, S. P., Kouveliotou, C., Fishman G. J., Meegan, C. A., & Paciesas, W. S. 1994b, in AIP Conf. Proc. 307, Gamma-Ray Bursts, ed. G. J. Fishman, J. J. Brainerd, & K. Hurley (New York: AIP), 172
Norris, J. P., et al. 1995, ApJ, 439, 542
Wood, K. S., et al. 1986, in AIP Conf. Proc. 141, Gamma-Ray Bursts, ed. E. P. Liang & V. Petrosian (New York: AIP), 4

© American Astronomical Society • Provided by the NASA Astrophysics Data System